COMPRESSIONAL WAVE POWER SPECTRUM FROM SEISMIC SOURCES

Ilkka Noponen

Helsinki University

Prepared for:

Advanced Research Projects Agency

31 October 1973

Security Classification

DOCUMENT CONTROL DATA - R & D AD 774027

(Security classification of title, body of abstract and indexing annotation must be entered when the overall report is classified)

1 ORIGINATING ACTIVITY *(Corporate author)*
Institute of Seismology, Univ. of Helsinki
Et.Hesperiankatu 4
SF-00100 Helsinki 10

2a. REPORT SECURITY CLASSIFICATION

2b. GROUP

3 REPORT TITLE
COMPRESSIONAL WAVE POWER SPECTRUM FROM SEISMIC SOURCES

4 DESCRIPTIVE NOTES *(Type of report and inclusive dates)*
Scientific. Interim.

6 AUTHOR(S) *(First name, middle initial, last name)*
Ilkka T.Noponen

6 REPORT DATE	7a. TOTAL NO. OF PAGES	7b. NO. OF REFS
31.10.1973	76	34

8a. CONTRACT OR GRANT NO	9a. ORIGINATOR'S REPORT NUMBER(S)
AFOSR-72-2377	ISRN 951-45-0272-8
b. PROJECT NO: AO 2131	
c. 62701D 2F10	9b. OTHER REPORT NO(S) *(Any other numbers that may be assigned this report)* AFOSR - TR - 74 - 0140
d.	

10 DISTRIBUTION STATEMENT
Approved for public release; distribution unlimited

11 SUPPLEMENTARY NOTES	12. SPONSORING MILITARY ACTIVITY
TECH, OTHER	United States Government American Embassy (EOARD) London, England

13. ABSTRACT

The power spectra of P wave signals are studied. Data from the 22 long period (LP) and short period (SP) sensors of the NORSAR array in Norway is used. For each type of sensor, the signals from all sensors are combined in an optimum way to produce average LP and SP spectra. Bias due to noise power is removed, the instrument responses are corrected for and the LP and SP spectra merged together. About 150 events are treated, of these the LP signals are analyzed for about 20 events. The earthquake and explosion spectra agree well with the predictions of analytical source models. The corner frequencies, where the power begins to decrease with increasing frequency, are roughly three times higher for explosions than for earthquakes of comparable magnitude (in the m_b range 5.0-6.0). This causes the low-frequency power level to be lower for explosions. At the frequency 0.3 Hz explosion signal power is typically 20 dB less than the power of signals from earthquakes with similar magnitude. Large and systematic regional variation is observed in the slope of spectra at frequencies above 2 Hz. This is interpreted to stem from variation of anelastic attenuation in the Earth. This large variation makes suspect the value of event classifiers employing energy at the higher frequencies of the P wave spectrum. Comparisons of power in the vicinity of the corner frequency may offer classification capability because the expected spectral differences are well demonstrated and the influence of attenuation during wave transmission is not yet prohibitive in the frequency range.

DD FORM 1 NOV 68 1473

Security Classification

14. KEY WORDS	LINK A		LINK B		LINK C	
	ROLE	WT	ROLE	WT	ROLE	WT
Norsar						
seismic discrimination						
P waves						
power spectrum						
beamforming loss						
signal-to-noise ratio						
noise bias correction						
corner frequency						
wave attenuation						
short period discriminants						
tectonic regions						

October 31, 1973

SCIENTIFIC REPORT No. 1

COMPRESSIONAL WAVE POWER SPECTRUM FROM SEISMIC SOURCES

JUNE 30,1972 - JUNE 29,1973

ILKKA NOPONEN

Institute of Seismology, University of Helsinki
Et.Hesperiankatu 4, SF-00100 Helsinki 10
Finland

SPONSORED BY

ADVANCED RESEARCH PROJECT AGENCY
ARPA ORDER No. AO 2131-1

16

ARPA Order No.: AO 2131-1
Program Code No.: 62701E 3F10 Project: AO 2131
Name of Grantee: University of Helsinki
Date of Grant: 72 JUN 30
Amount of Grant $22,640.00
Grant Number: OSR-72-2377
Grant Completion Date: 74 DEC 31
Project Scientist: Dr. Ilkka Noponen
Title of Grant: "SEISMIC WAVE PROPAGATION UNDER THE BALTIC SHIELD"

ISBN 951-45-0272-8

FOREWORD

The work reported in this document was performed at Institute of Seismology, University of Helsinki under the grant OSR-72-2377. The author visited the Norwegian Seismic Array Data Center in Kjeller, Norway during the first half of the period covered by this report, and the significant help received from the NORSAR staff is gratefully acknowledged. The author could benefit from innovative discussions, in particular with the staffs of the Seismic Array Analysis Center in Alexandria, Virginia and of the Lincoln Laboratory, MIT, Boston, during a short trip to the United States. Thanks are due to several very helpful persons met during that visit.

TABLE OF CONTENTS

LIST OF ILLUSTRATIONS

I. INTRODUCTION

In this work the power spectra of P waves from seismic events recorded at the NORSAR large seismic array in Norway have been observed. An objective of the study is to compare the shapes of spectra from earthquakes and explosions, in the hope of finding stable differences between the two types of events, which would aid in the classification of seismic events. Other objectives are to estimate parameters of the seismic sources by comparing the observed spectra to predictions made using simplified source models[1,2,3,4,5,6] and to observe regional variations of spectra which could be attributed to propagation path effects.

In this report observations of P-wave spectrum in the frequency range 0.03 and 6 Hz are described. Observations in a broad frequency range are also reported in references[7,8]. Wyss, Hanks and Liebermann[7] reported the greatest differences between earthquake and explosion spectra to be found at low frequencies, where the signal-to-noise ratio (SNR) for weak events is poor.

For classification, differences in the frequency range 0.5-4 Hz which has a good SNR would be most valuable. That frequency range has been used for computing single numbers('discriminants') which describe the relative levels of the high and low frequency energy of a spectrum[9,10,11,12,13,14]. In this work such a single parameter is also defined and computed for a number of spectra. The value of such parameters for classification is still unclear.

In estimating the spectrum of a P wave using a large seismic array an optimum method for combining data from all sensors should be used. The NORSAR short period sensors give 132 paral-

lel recordings from each signal. Each of these differs slightly from all the others, while the noise at the different sensors is assumed to be completely uncorrelated. To make use of all sensors and to arrive into a single power spectrum, a basic decision is whether one should average over the signals themselves (beamforming) prior to computing the power spectrum, or whether the average over the power spectra computed for each single sensor should be used (spectraforming).

Lacoss and Kuster[15] showed that (a) the spectra computed by spectraforming and beamforming differ from each other ever in the absence of noise and that (b) in case of weak signals the selection of a proper method is of importance in extracting the signal from the noise. The delays required for the delay-and-sum

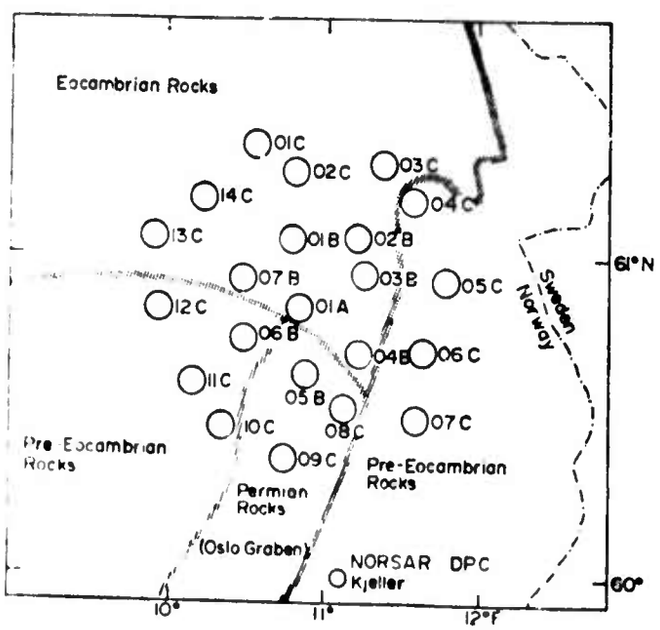

Fig. I.1. NORSAR array configuration. The 22 subarrays are shown. Each subrray is equipped with 6 vertical short-period sensors and one 3-component long-period seismometer.

operation in beamforming may be poorly known for a weak event and this may cause unpredictable and large beamforming losses at the higher signal frequencies. This is a strong argument against the use of beamforming in computing power spectrum at the the higher frequencies. If no beamforming losses would exist, beamforming would be the best method for extracting the signal spectrum from the noise, but the losses worsen its performance.

All spectra presented in this report are computed using a combination of beamforming and spectraforming. We averaged 22 power spectra computed for the 22 subarray beams from the NORSAR subarrays. Each subarray beam was formed by averaging signals with suitable delays, recorded by 6 sensors within a region of 7-8 km in diameter. The geometry of NORSAR is shown in fig.I.1.

In terms of stability, beamforming loss and computing time this was considered a good compromise. In Appendix 1 measurements of SNR and beam losses from events in Central Asia are presented, and the reasons for the selection of the procedure of averaging subarray beams are presented in more detail. These measurements have been published earlier[16].

In extracting the spectraformed signal from the noise the most important operation is the subtraction of an estimate of noise power from the signal power. With certain assumptions on noise, the expected value of the remainder is equal to true signal power in the frequency band considered[15]. As noted also by Linde and Sacks[17], this removal of bias due to noise is of prime importance when observing frequencies out of the dominant signal frequency. The noise-correction is described in detail in Appendix 2.

In collecting data it was tried to include events from various

tectonic provinces and to observe earthquakes in the vicinities of nuclear test sites. All included earthquakes were shallow, as a rule maximum depth limit of 50 km was used, but including some events in the depth range 50 to 70 km. The depth 70 km corresponds to the supposed lower boundary of the low-attenuation, high-Q lithosphere. Initially only events in the magnitude range 5.0 - 6.0 m_b were analyzed, because a homogeneous data set was desired. That also is the optimum observation range if both short and long period sensors are used. Later a wide magnitude range was covered. A list of all included events is given as Appendix 3.

The magnitudes of events quoted in this report are P wave magnitudes (m_b) given by the (U.S.)National Earthquake Information Center (NEIC), formerly referred to with abbreviations USCGS and NOAA. Whenever the magnitude is given from another agency or is computed from other waves, this is indicated.

In computing a power spectrum using long period sensors, signals from the 22 vertical LP sensors, one in each subarray, are beamformed (summed with delays), a signal section 96 seconds long and beginning 1-2 sec prior to the onset time of the P waves is Fourier transformed and the absolute value of the transform is squared. Bias due to noise is removed by subtraction of noise power. The spectra presented in the figures of this report are smoothed over a bandwidth of 0.021 Hz. In computing a power spectrum using short period sensors, the combined beamforming/spectraforming procedure described above was used. Signal sections of 6.4 or 12.8 seconds were used. The noise-corrected power spectra presented in figures were smoothed over a bandwidth of 0.313 Hz.

II. GENERAL SHAPE OF SPECTRA

In this chapter the general shape of earthquake and explosion spectra is described using spectra computed from shallow earthquakes and explosions in Eastern Europe, Western and Central Asia, at the western coast of North America and at the Aleutian Islands. By combining measurements made with long and short period (LP and SP) sensors the shapes of the P wave spectra within the frequency range 0.03 to 6.0 Hz could be studied. In several cases, however, the signal-to-noise ratio (SNR) was not sufficient below the frequency 0.3 Hz for the signal spectrum to be extractable from the noise. In addition to the observations reported in this chapter for a number of events only the signals recorded by the SP sensors were spectral analyzed. Those observations will be described in the next chapter.

In fig. II.1 are shown displacement power spectra for 6 earthquakes in Central Asia. The spectra are corrected for the NORSAR SP and LP instrument responses. The spectra shown are selected from a suite of 13 spectra as those which had the best SNR in the long period range. This will give a somewhat biased view, but a low signal power was not the only reason for rejecting spectra. The large variation in the background noise level, in some cases caused by interfering events, also influenced the detection of LP P waves.

The general impression is that for these events having magnitudes 5.2 - 6.0 (m_b) the spectra follow the prediction of Aki[4]. The power level is roughly constant at frequencies below 0.2 - 1.0 Hz, at higher frequencies the power decreases rapidly and almost monotously with increasing frequency. The variations in the relative levels of high and low frequency energy are large. The shocks 101, 102, 105 and 111 all have the magnitude 5.6(m_b).

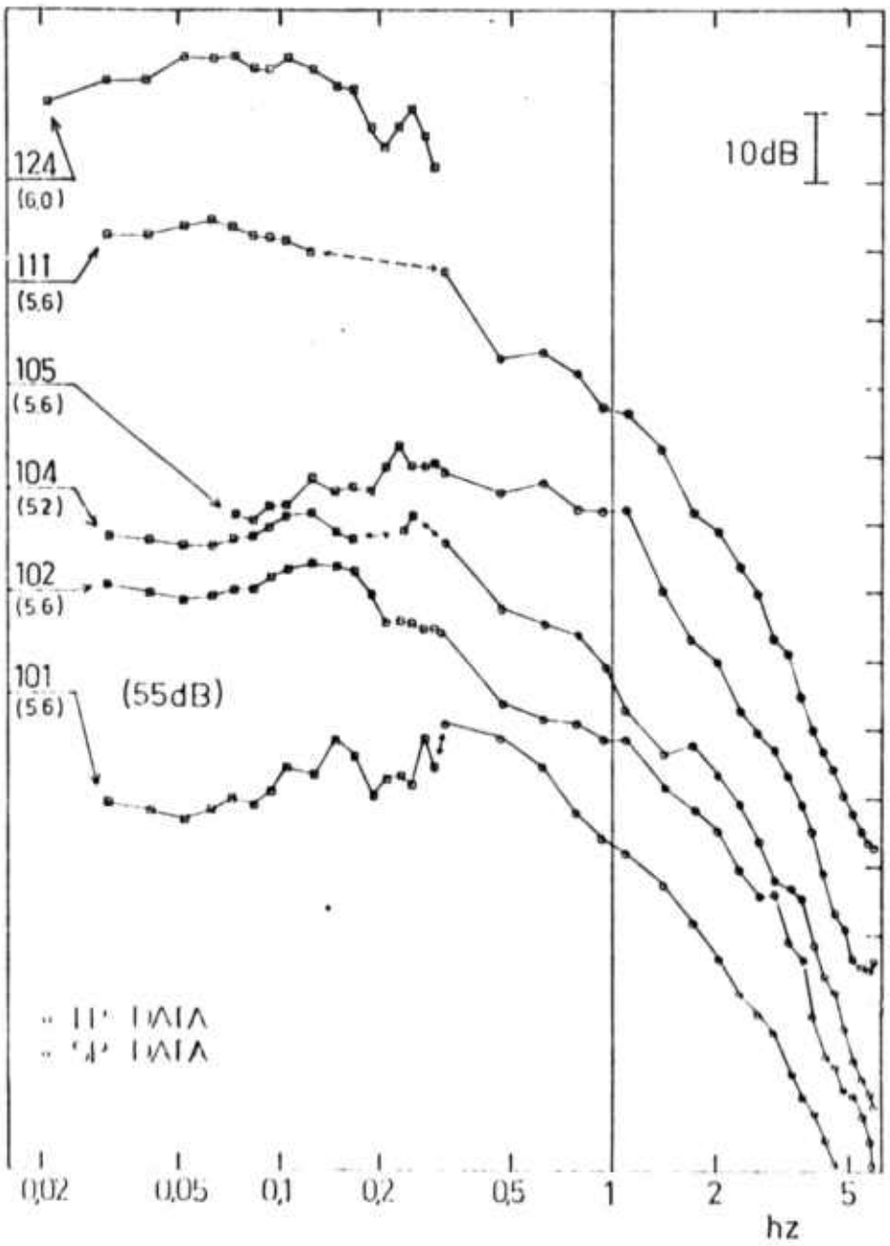

Fig. II.1. Earth displacement power spectra of earthquakes in Central Asia. The spectra are displaced by steps of 15 dB for clarity. Short horizontal lines at left margin show for each spectrum the level of 55 dB over power density 1 nm^2/Hz. Magnitudes are given in parentheses.

This is reflected in their equal levels of power at the frequency 1.0 Hz, where the measurement for the m_b magnitude is made. But their long period power levels vary by 20 dB, or by one order of magnitude.

This variation is coupled with the variation of the corner frequency, where the spectral power begins to fall off with increasing frequency. It ranges from 0.2 to 1.0 Hz for these spectra. If the conclusion of Brune[5] (1970), that the corner frequency of S wave spectrum is inversely proportional to the radius of the source fault, can be applied to P waves the source radii vary by a factor of five, even within the four shocks with magnitude 5.6.

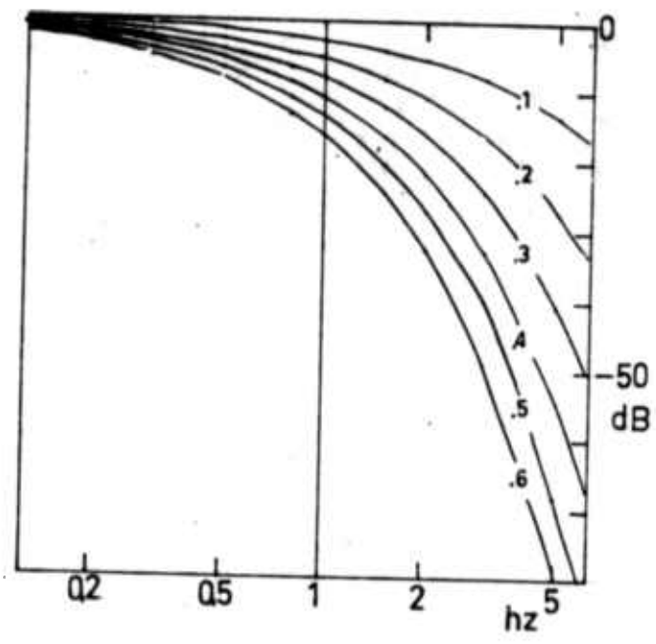

Fig. II.2. The amount of attenuation as a function of frequency for different values of the parameter t .

In fig. II.2 the effect of non-elastic attenuation is shown for various values of the frequency-independent quality factor Q.

The curves show the magnitude of a factor $\exp(-\pi f t^*)$ with t^* as the parameter. The quantity t^* is

$$t^* = \int_0^T \frac{dt}{Q} \qquad \text{and} \qquad \bar{Q} = \frac{t}{t^*} \tag{2.1}$$

where t is the travel time and $\bar{Q}$ is the apparent average Q along the rav path. The available scanty evidence on t^* along the path Central Asia-NORSAR suggests a value less than 0.3[18,19]. Any value of t^* between 0 and 0.3 does not change the conclusions on the existence and location of the corner frequencies in fig. II.1.

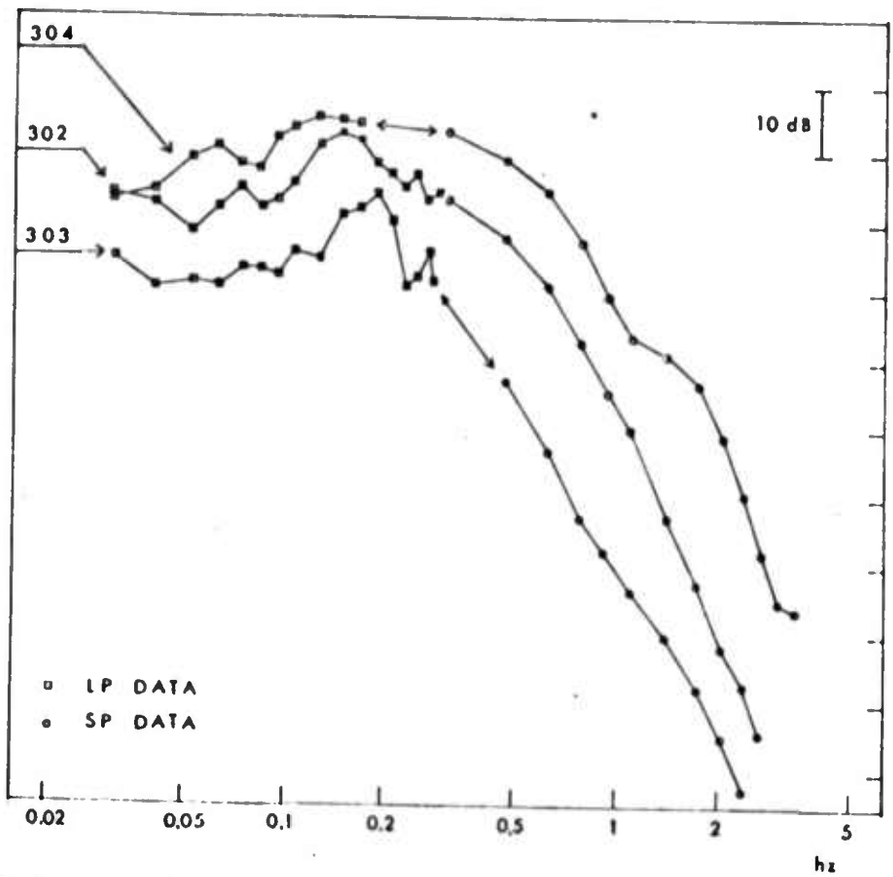

Fig. II.3. Earth displacement power spectra of earthquakes at the western coast of North America. The spectra are displaced in steps of 15 dB for clarity. Short horizontal lines at left margin show for each spectrum the level of 55 dB above power density 1 nm^2/Hz. Magnitudes of events are given in parentheses

In fig. II.3 are presented spectra from three shallow earthquakes at the western coast of North America in the magnitude range 4.8 - 5.6 m_b. The spectra have a somewhat more peaked character than the Central Asian spectra. It has to be noted, however, that the total response of the earth to a wave sent from a source modifies the origina.. spectrum, particularly in case of the long period waves. An example of this is the interference of the pP and PcP waves with the P wave. In case of these events, both of these later phases arrive within the 96 sec long window of analysis.

The corner frequencies vary from 0.2 to 0.5 Hz. The slope of spectra at high frequencies is clearly larger than that of the Central Asian spectra. This is most probably due to a difference in the total effect of the non-elastic attenuation along the two ray paths.

In fig. II.4 the spectra of 9 explosions in Eastern Kazakh are shown. No signal power could be extracted from the LP signals below the frequency 0.3 Hz. Whenever observable, the power at frequencies below 1.0 Hz is rather constant. Comparison with fig. II.2 shows that if these spectra were corrected for attenuation taking t^* to be 0.2, in all cases the power would be constant below 1.0 Hz or have a maximum around that frequency. The value $t^* = 0.2$ corresponds to $\bar{Q} = 2190$.

Seggern and Blandford[6] predicted the far-field P wave spectrum from underground explosions to be flat below a corner frequency depending on the yield, with a possible overshoot at the corner frequency. The picture emerging here is not in disagreement with their prediction. The frequencies of the maxima observed range from 0.5 to 1.0 Hz (events 512, 514 and 516) which fits well with the prediction of Seggern and Blandford for explosion yields 50-100 kt. These events have been estimated to lie within the yield limits 20 to 200 km[20].

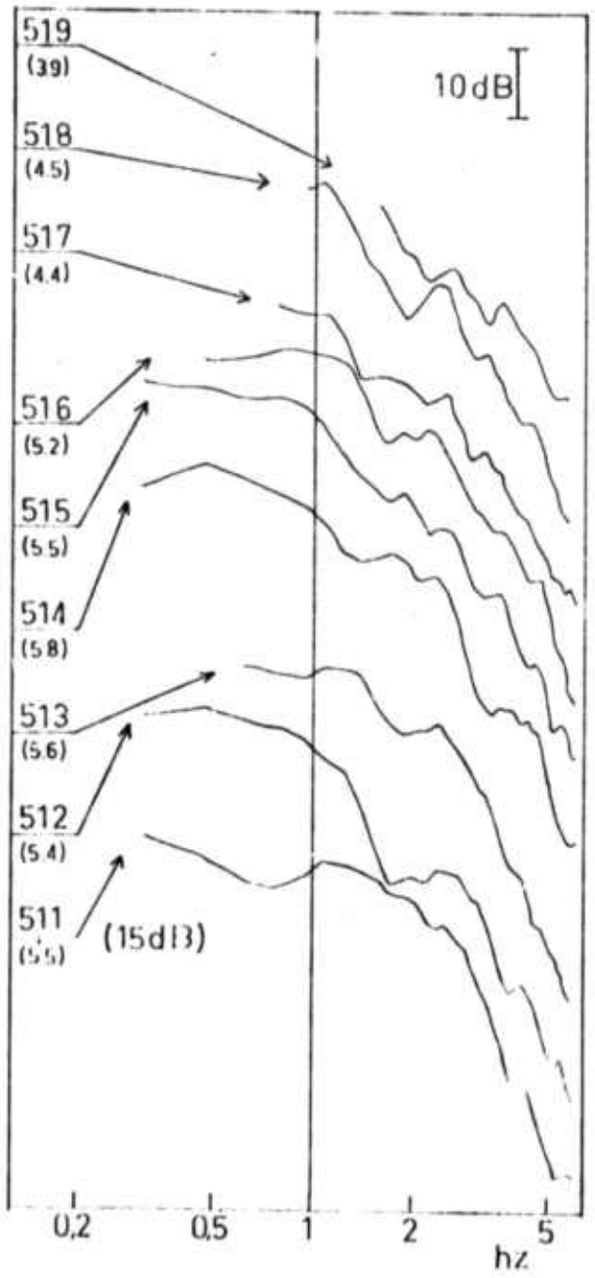

Fig. II.4. Earth displacement power spectra of underground explosions in Eastern Kazakh. The spectra are displaced in steps of 15 or 25 dB for clarity. Short horizontal lines at left margin show for each spectrum the level of 15 dB above power density 1 nm^2/Hz. Magnitudes of events are given in parentheses.

One would apparently prefer to have observations at lower frequencies to make certain the detection of a corner frequency. There is unfortunately an inherent difficulty. As soon as the increase of signal power with decreasing frequency begins to level off, the signal is overwhelmed by the even more steeply increasing noise and becomes impossible to measure, even with the capabilities of a large array. Further, when the yield increases, the corner frequency decreases coming to a region of worse SNR, which offsets the general improvement in the SNR.

These difficulties are somewhat overcome in observing the spectra of the presumed explosions in Western Russia, because they lie closer to NORSAR, at distances 15°-20°. In fig. II.5 are shown the spectra of 7 events in Western Russia with magnitudes ranging from 3.2(given by NORSAR) to 5.5. The larger events of this set have relatively more energy at low frequencies than the smaller events. LASA array locates the event WR2 to Western Kazakh, rather than to Western Russia. It is thus not comparable with the other events. Its LASA magnitude is 3.8.

In case of the events WR3 and WR4 with magnitudes 4.6 and 4.5 (as given by LASA) there is a very slow decrease of power with increasing frequency in the observation range 0.5 to 3.3 Hz. Taking for these ray paths in the upper mantle a $\bar{Q}$ less than 1500, a correction for the effect of attenuation will result into virtually constant power levels in the observed frequency range. This would mean the corner frequencies to be above 2 Hz.

The three events with magnitudes above 5.0 have spectra which even with a reasonable correction for attenuation display corner frequencies around or below 1.0 Hz. This is in agreement with the observations from E.Kazakh explosions. The event WR1 with NORSAR magnitude 3.2 shows a maximum of power at 2.0 Hz.

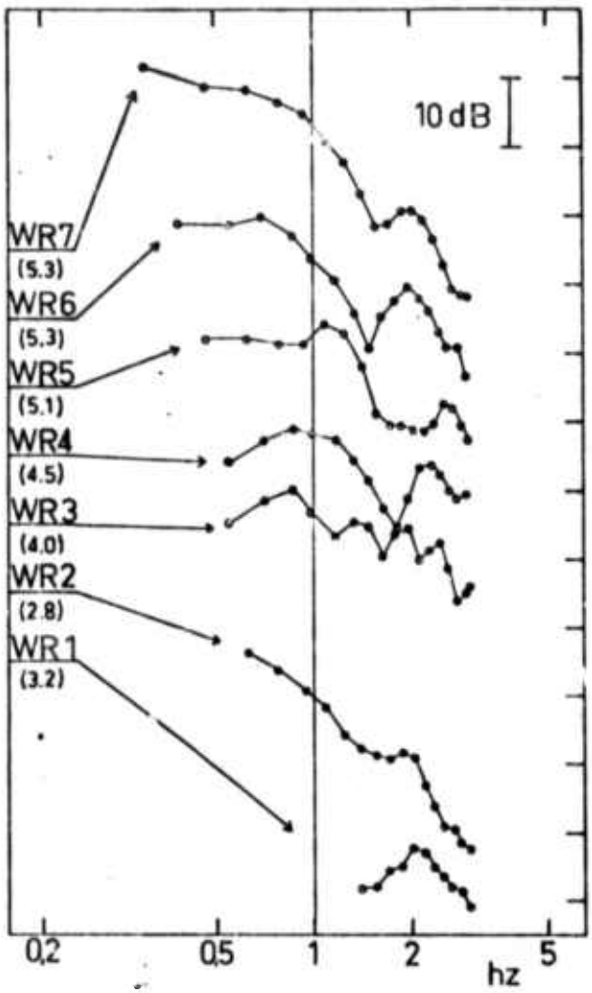

Fig. II.5. Earth displacement power spectra of presumed underground explosions in Eastern Europe. The spectra are displaced in steps of 10 dB for clarity. Short horizontal lines at left margin show an equal power level for each event. Magnitudes of events are given in parentheses.

For the purpose of observing the explosion spectrum at frequencies well below the corner frequency, long period P signals from the Cannikin explosion with magnitude 6.8 at Aleutian Islands were spectral analyzed (event code 122). In fig. II.6 its spec-

strum is shown with the spectrum of an shallow earthquake at a nearly same location. The LP signals from these two events are shown in fig. II.7. The explosion is 1-? magnitude units larger than those presented in previous figures and it seems that the corner frequency is between 0.2 and 0.3 Hz.

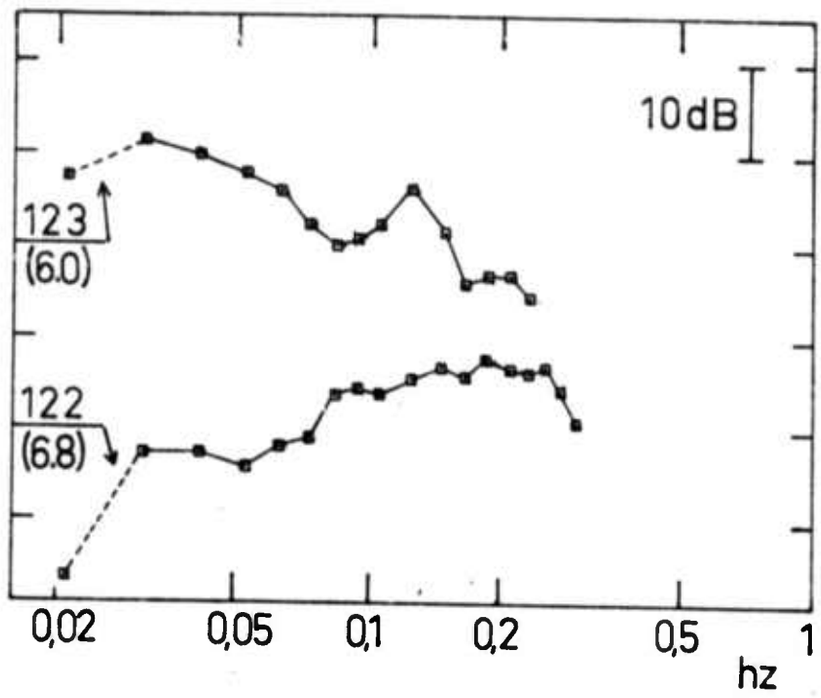

Fig. II.6. Earth displacement power spectra for an underground explosion at Aleutians (code 122) and for a large earthquake at nearly same location (code 123). The earthquake spectrum is shifted up by 20 dB for clarity. Short horizontal lines at left margin show for each spectrum the level of 55 dB above power density 1 nm^2/Hz. Magnitudes of events are given in parentheses. The lowest frequency band is not included in frequency smoothing.

This range fits excellently with the corner frequency 0.26 Hz, which has been predicted[6] for an explosion of 5 Mt (the probable yield of this explosion[20]).

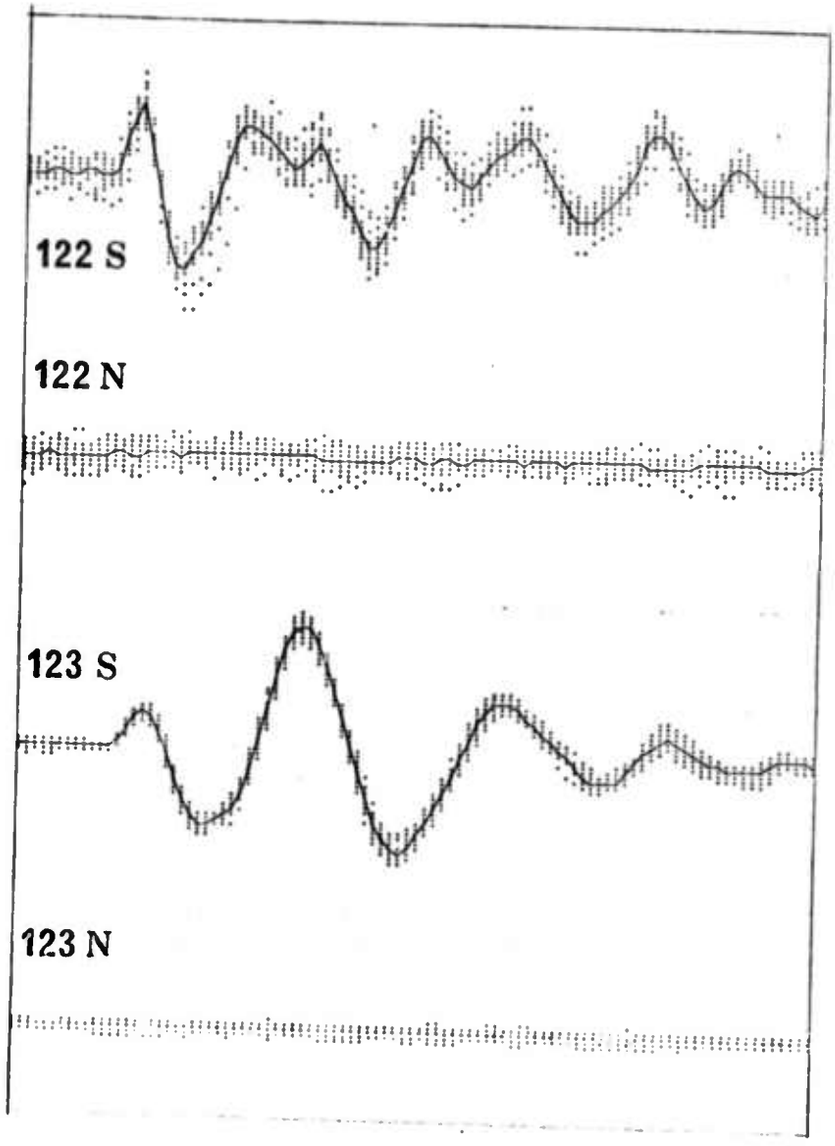

Fig. II.7. The LP signals from the Cannikin explosion (code 122) and a large earthquake in Aleutians (code 123). The continuous lines represent LP beams aimed towards the events, the dots around these represent the single channel recordings. S and N stand for signal and for a sample of preceding noise, respectively. The earthquake signal is larger than the explosion signal on the original records. Note the good coherence of LP signals when S/N ratio is large (event 123).

The decrease of power with decreasing frequency could be entirely caused by the crustal transfer function at the source. The transfer function is dominated by the P/pP interference. Scaling the transfer function for a shallow explosive source in a continental crust computed by Fuchs[21] to the present source depth 2 km, we would expect the power at 0.05 Hz to be 20 dB less than at 0.35 Hz. This is sufficient to explain the slope of the present spectrum, and there is no objection to a flat explosion spectrum at low frequencies predicted when the effect of the free surface is absent[6].

The large ripples at varying frequencies superposed on the general trend of the explosion spectra in figs II.4 and II.5 are also explained as successive bands of constructive and destructive interference between P and pP. The greater depth of the earthquakes causes these bands to be narrower in the earthquake spectra and they are smeared out in the frequency smoothing. The pP phase may also remain outside the time window taken for analysis.

In fig. II.8 the corner frequencies read from the earthquake and explosion spectra shown in figures II.1, II.4 and II.5 are plotted as function of magnitude. Earthquake corner frequencies are roughly three times smaller than those of explosions. The prediction for explosion corner frequency as a function of yield made by Seggern and Blandford[6] is also plotted to the figure, assuming the yield Y and seismic magnitude m_b being connected by equation

$$\log Y = m_b - 3.9$$

as seems reasonable for explosions in hard rock[33]. Considering the uncertainties in reading the corner frequency from a spectrum and in the magnitude-yield relationship, the fit is not bad and indicates that corner frequencies are really observed.

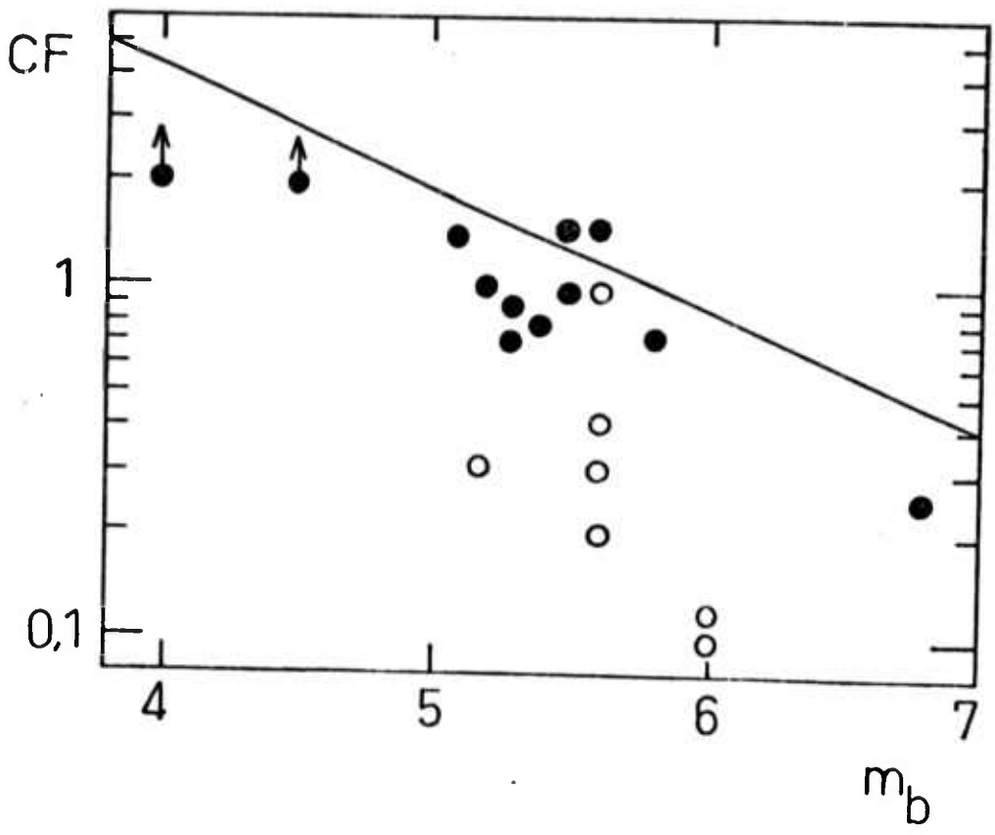

Fig. II.8. Corner frequencies (CF) in Hz, read from spectra of earthquakes (open circles) and explosions (filled circles). The line represents the predicted corner frequency for explosions in hard rock.

III. SPECTRA FROM DIFFERENT REGIONS

In this chapter the shapes of spectra from events at different regions are compared. Only data recorded by short period sensors is presented because of the often poor SNR of P waves at low frequencies. Because different regions were observed to have significantly different shapes of spectra, the events are grouped geographically.

The presented spectra are not displacement spectra, as in the previous chapter, but acceleration spectra. Response-corrected power at each frequency has been multiplied by ω^4, and the power scale in figures is in dB, or equivalent to $10 \cdot \log_{10}(P/P_0)$ where P is the spectral power and P_0 is some constant reference level. The spectra within each geographical group are normalized to equal total power (at the SP sensor system output) and the spectra are averaged as described in app. 2. The individual spectra and the average are shown in figures. Frequency smoothing over a bandwidth of 0.31 Hz is done.

The events in this chapter are usually identified only by indicating the event set to which they belong. Information on individual events arranged according to the event sets is given in app. 3. Figures III.1 and III.2 indicate the locations of the events and event sets. All earthquakes included to analysis are shallow, i.e. have reported depths less than 70 km, and most have reported depths less than 50 km. In some cases the depth is difficult to verify, but these events are few and generally at regions where intermediate or deep shocks are not known to occur.

The 15 events scattered over Eastern Asia, from Kamchatka to China, show a large variation of spectral shapes (fig. III.3).

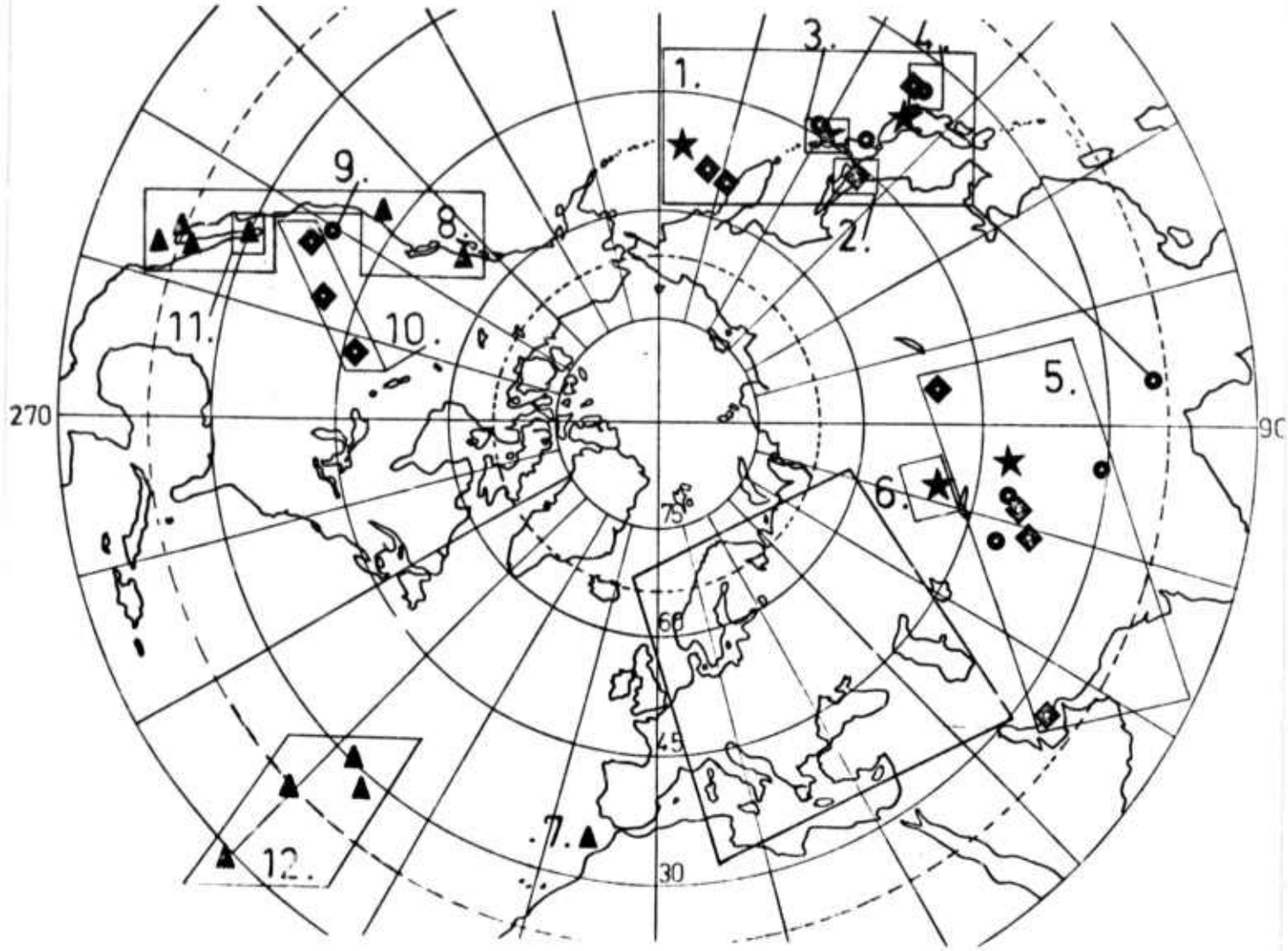

Fig. III.1. Analyzed events excluding those in Europe. The events are divided into following event sets (numbers refer to figure): 1. EASTERN ASIA, 2. SAKHALIN, 3. KURILES,4. SOUTH OF HONSHU, 5. CENTRAL ASIA, 6. EASTERN KAZAKH(explosions), 7. GIBRALTAR, 8.WEST COAST OF NORTH AMERICA, 9. NEVADA (explosions), 10. UTAH/DAKOTA, 11. GULF OF CALIFORNIA, 12. MID-ATLANTIC RIDGE. The different symbols indicate relative high-frequency contents of spectra, estimated by the LTM measure. When several events fall to a nearly same location, their average LTM value is plotted. Triangle: LTM<0, square: 0.0<LTM<0.4, circle: 0.4<LTM<0.7, asterisk LTM>0.7.

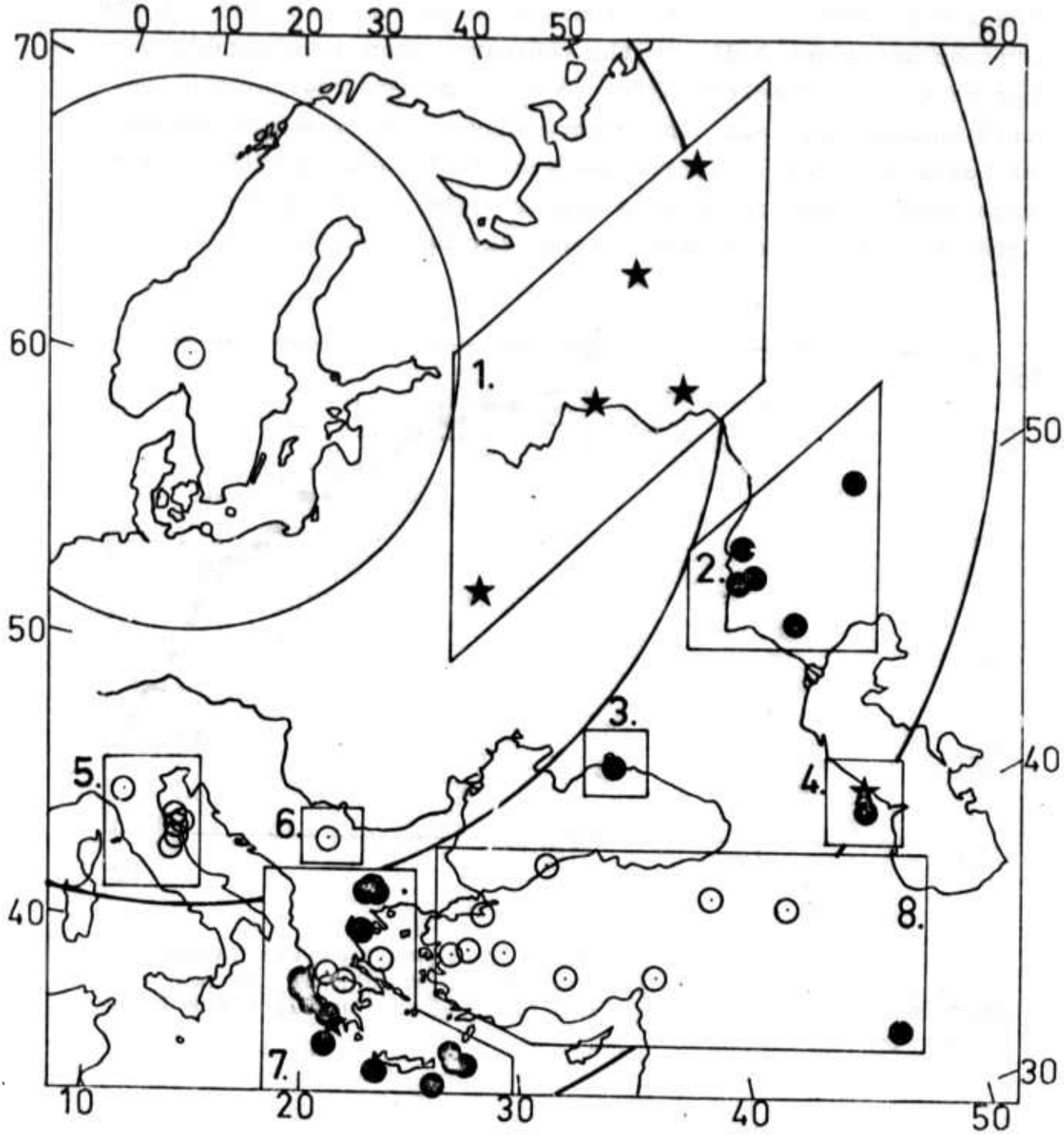

Fig. III.2. Events in Europe. The events are divided into following event sets (numbers refer to the figure): 1. WESTERN RUSSIA (presumed explosion), 2. WESTERN KAZAKH (presumed explosion), 3. CRIMEA, 4. EASTERN CAUCASUS, 5. ITALY, 6. YUGOSLAVIA, 7. GREECE, 8. TURKEY. The different symbols indicate relative high-frequency contents in spectra, estimated by the LTM measure. Open circle: LTM<0.4, filled circle: 0.4<LTM<0.9, asterisk LTM>0.9.

The r.m.s. deviation of the individual spectra (in dB) from the average surpasses 8 dB. On the contrary, when a comparable number of events is selected from a small source region, the spectral shapes vary less. The events in very small source regions at Sakhalin(fig.III.4), Kuriles(fig.III.5) and Japan(fig.III.6) each show rather homogeneous spectra, the r.m.s. deviations from the respective averages generally being below 3 dB.

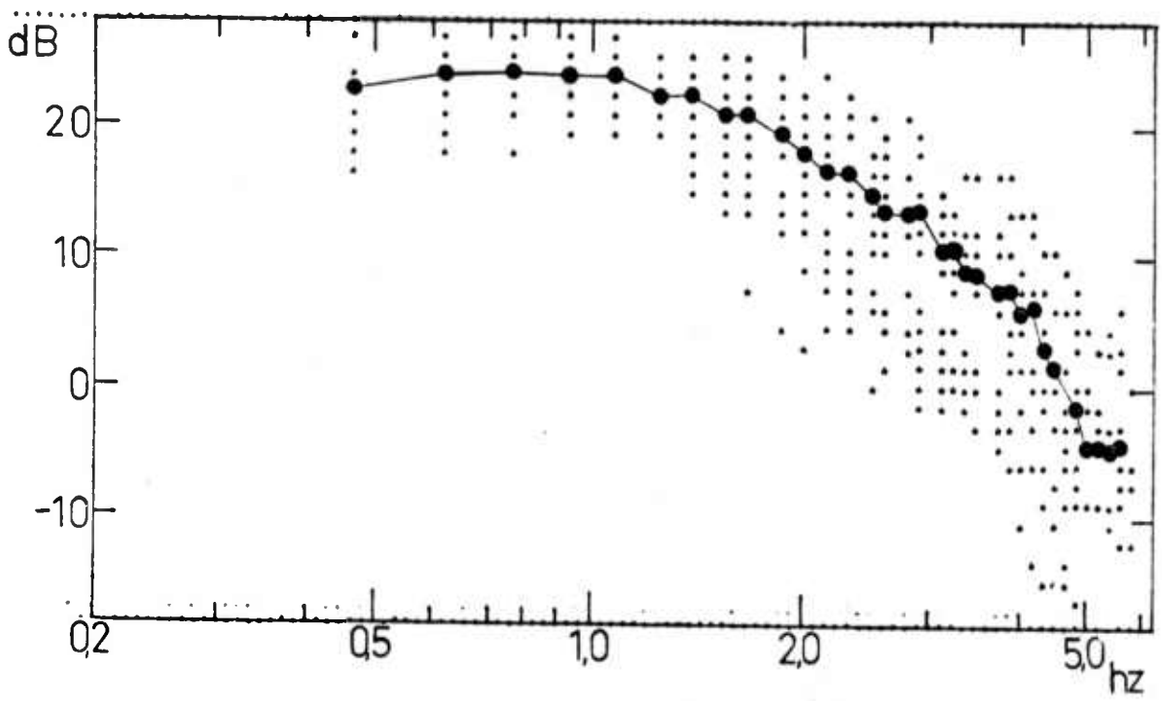

Fig. III.3. Normalized acceleration power spectra (asterisks) with average (circles) of the 15 shocks of the set EASTERN ASIA in magnitude range 5.0-6.3 m_b and distance range 60 to 78 degrees.

The spectra recorded from SAKHALIN differ clearly from the KURILES spectra in their lower high frequency energy contents. One possible explanation for the difference is a difference in

the nonelastic attenuation along the respective wave paths. Such variations can explain why the EASTERN ASIA set with widely dispersed events displays a larger variation of spectral shapes than the more localized event sets. The magnitude also influences the relative amounts of high- and low-frequency energy, as is observed for earthquakes in figs III.4 and III.5 (SAKHALIN, KURILES) and for underground explosions in figs III.6 and III.7.

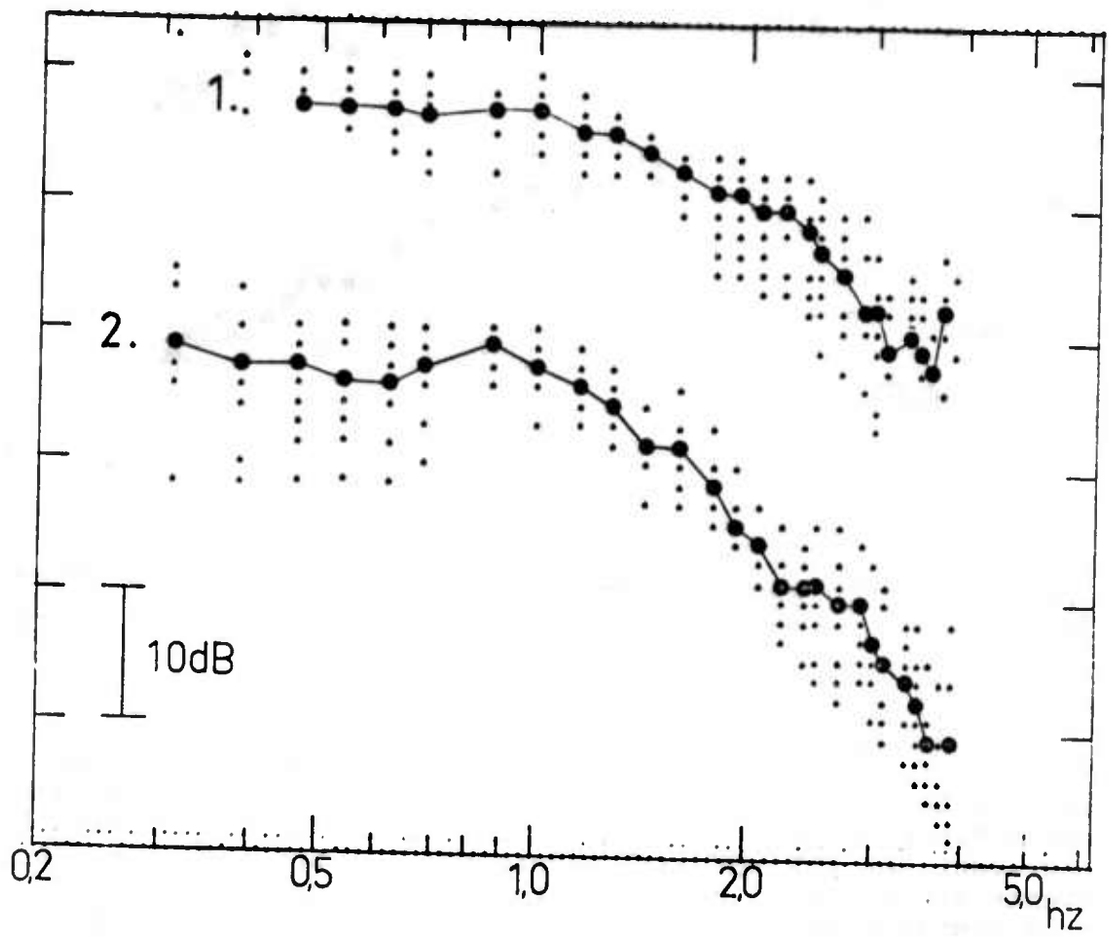

Fig. III.4. Normalized acceleration power spectra (asterisks) with averages (circles) of quakes in the event set SAKHALIN. All quakes occured within a 50 km radius from 46.5 N 141.1 E, at a distance of 65 degrees from NORSAR. (1) The 10 shocks in magnitude range 4.1-4.9 m_b. (2) The 10 shocks in magnitude range 5.0-5.9 m_b.

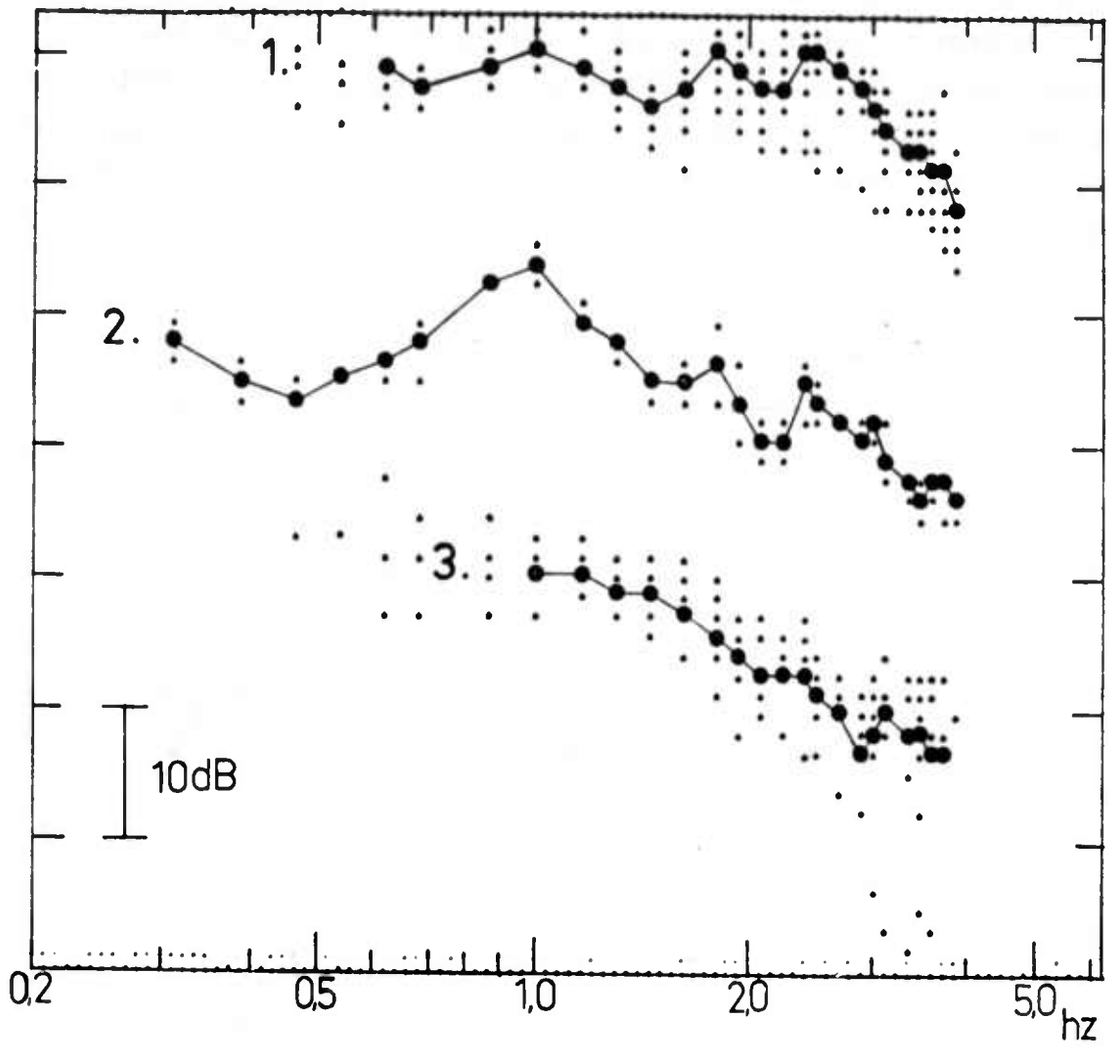

Fig. III.5. Normalized acceleration power spectra (asterisks) with averages (circles). (1) The 10 shocks of the event set KURILES in magnitude range 4.3-4.9. (2) The 2 shocks of the event set KURILES with magnitudes 5.7 and 6.0. The KURILES events are all within a 50 km radius from 44.7 N, 149.3 E, at a distance of 69 degrees from NORSAR. (3) The 9 events of the event set SOUTH OF HONSHU in the magnitude range 3.9-5.2m_b. The events are within a 50 km radius from 33.2 N, 141.0 E, at a distance of 78 degrees.

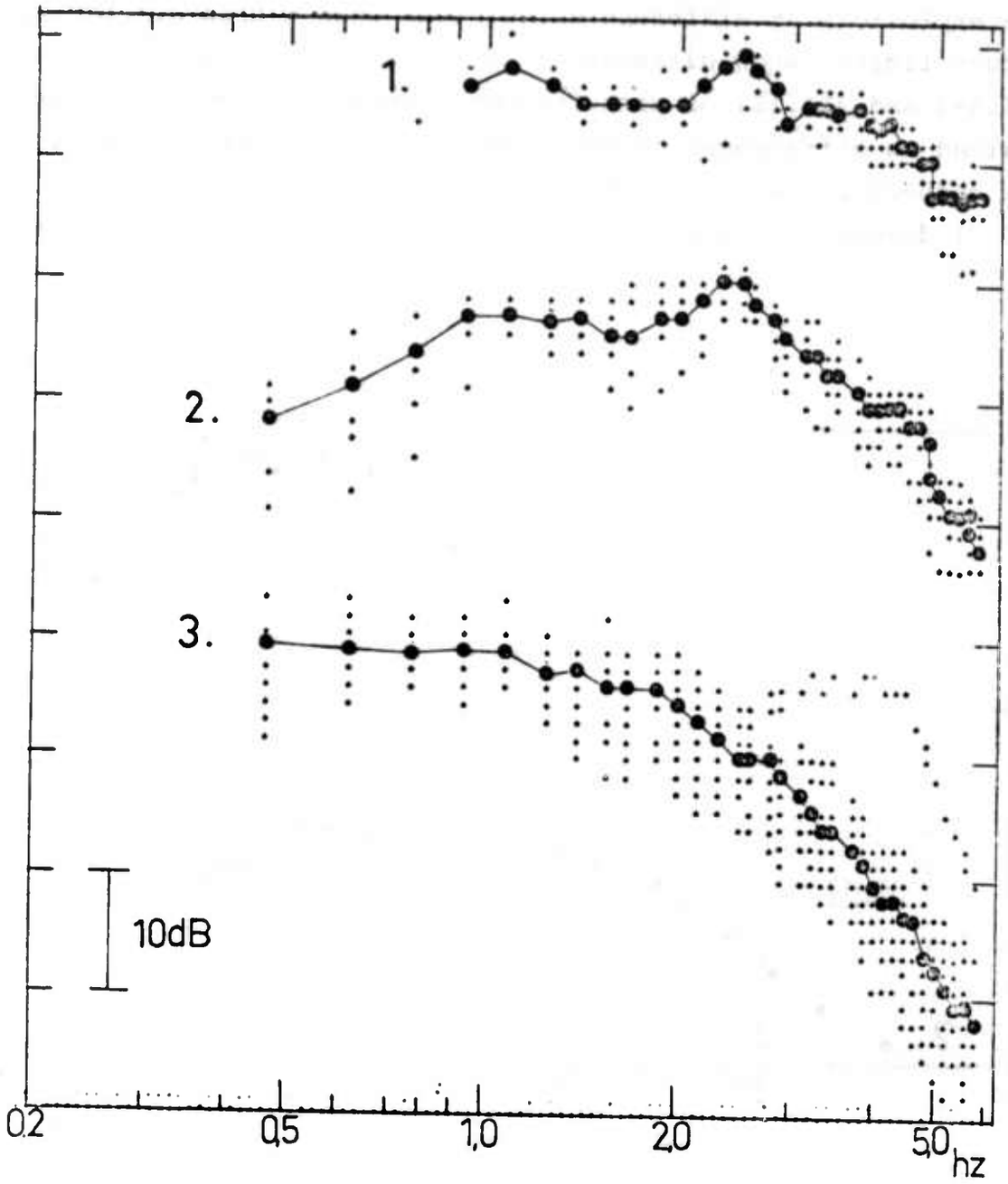

Fig. III.6. Normalized acceleration power spectra (asterisks) with averages (circles). (1) 3 explosions of the event set EASTERN KAZAKH in magnitude range 3.9(NORSAR) - 4.4 m_b. (2) 6 explosions of the same event set in the magnitude range 5.2 - 5.8 m_b. EASTERN KAZAKH is a small source region at a distance of 38 degrees from NORSAR. (3) The 15 shocks of the event set CENTRAL ASIA in the magnitude range 5.0 - 6.0 m_b and distance range 36-56 degrees.

The explosions at different sites, even when within similar magnitude limits, show differences in the relative amounts (figs III.6-8 and III.12) of high-frequency energy. These can be explained as differences in the nonelastic total attenuation at the respective ray paths. Explosions in Western Russia(fig. III.7) display a minimum at frequency 1.5 Hz, which appears as

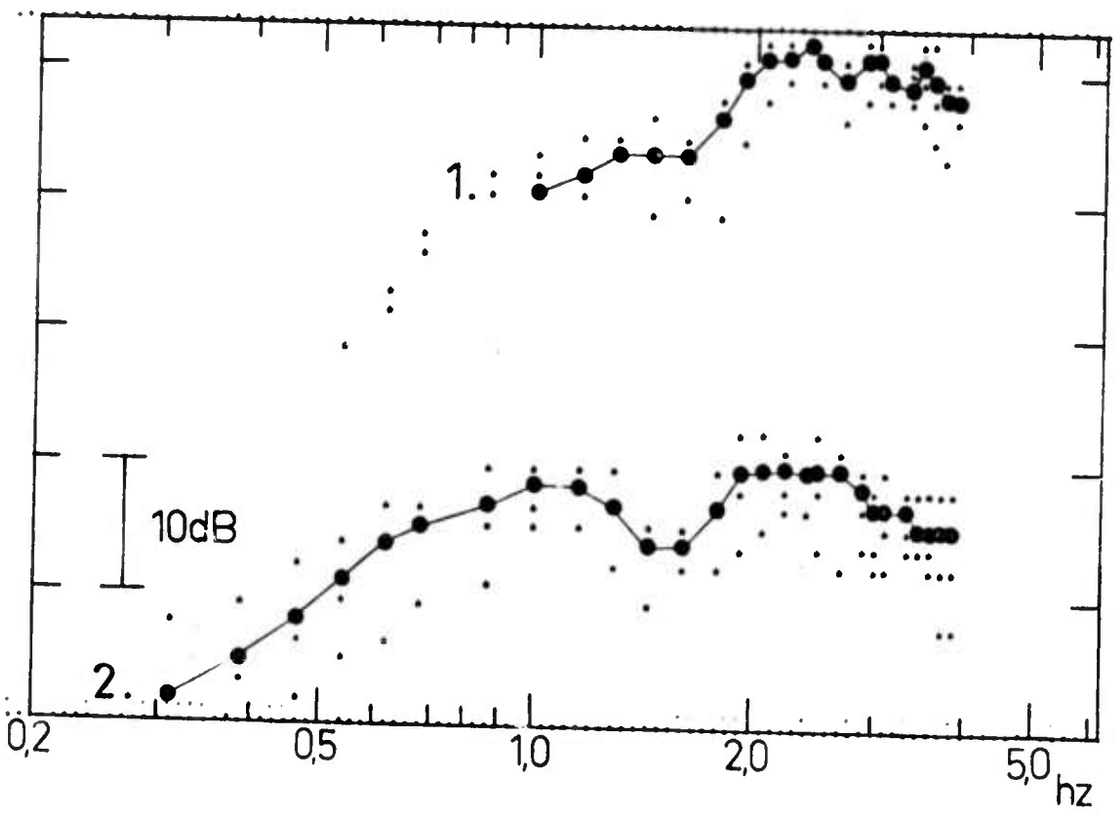

Fig. III.7. Normalized acceleration spectra (asterisks) with averages (circles) of presumed explosions in the event set WESTERN RUSSIA. (1) 3 events in the magnitude range 3.2(NORSAR) - 4.5 m_b and distance range 17-20 degrees. (2) 3 events in the magnitude range 5.1-5.3 m_b and distance range 18-25 degrees.

a minimum also in displacement spectra. The explosion spectra can be compared to earthquake spectra at certain regions where explosions and earthquakes occur at relatively close distances. Comparison between EASTERN KAZAKH explosions and CENTRAL ASIA earthquakes indicates clearly differing spectral shapes (fig. III.6). This is disturbed somewhat by the single highly anomalous earthquake in Sinkiang (code 229 in app. 3). That event is not included into averaging over earthquake spectra in fig. III.6. It will be further discussed later. The average explosion spectrum has a power ratio between 0.5 and 5 Hz ($P_5/P_{0.5}$) 20 dB larger than the corresponding ratio for the earthquakes, excluding event 229. but this clear difference does not occur for the other explosion sites. The WESTERN KAZAKH presumed explosions have a spectral shape very similar to the near-by presumed earthquakes at Crimea and Eastern Caucacus (fig.III.8). For the NEVADA explosions the large variation of spectra from earthquakes in southwestern North America makes any unambiguous comparison difficult. The presumed explosions in WESTERN RUSSIA have very strong high-frequency energy, but no near-by earthquakes exist for comparison. The quakes at Mid-Atlantic ridge and at western coast of North America have spectra which are very deficient at high frequencies when compared with spectra from events in Central Asia and Eastern Asia which are at comparable distances, respectively (figs III.3, III.6 and III.11). The large scatter and apparent increase of power at high frequencies from certain event regions (figs III.10-12) is probably due to the very weak high-frequency signal energy from those regions. At the high-frequency end of the observed spectral range the assumption of noise stationarity made in the noise-correction procedure described in app. 2 is apparently incorrect (gusts of wind, cultural noise) and the confidence limits computed for noise are too narrow. Thus the noise can accidentally influence estimation of weak high-frequency signals.

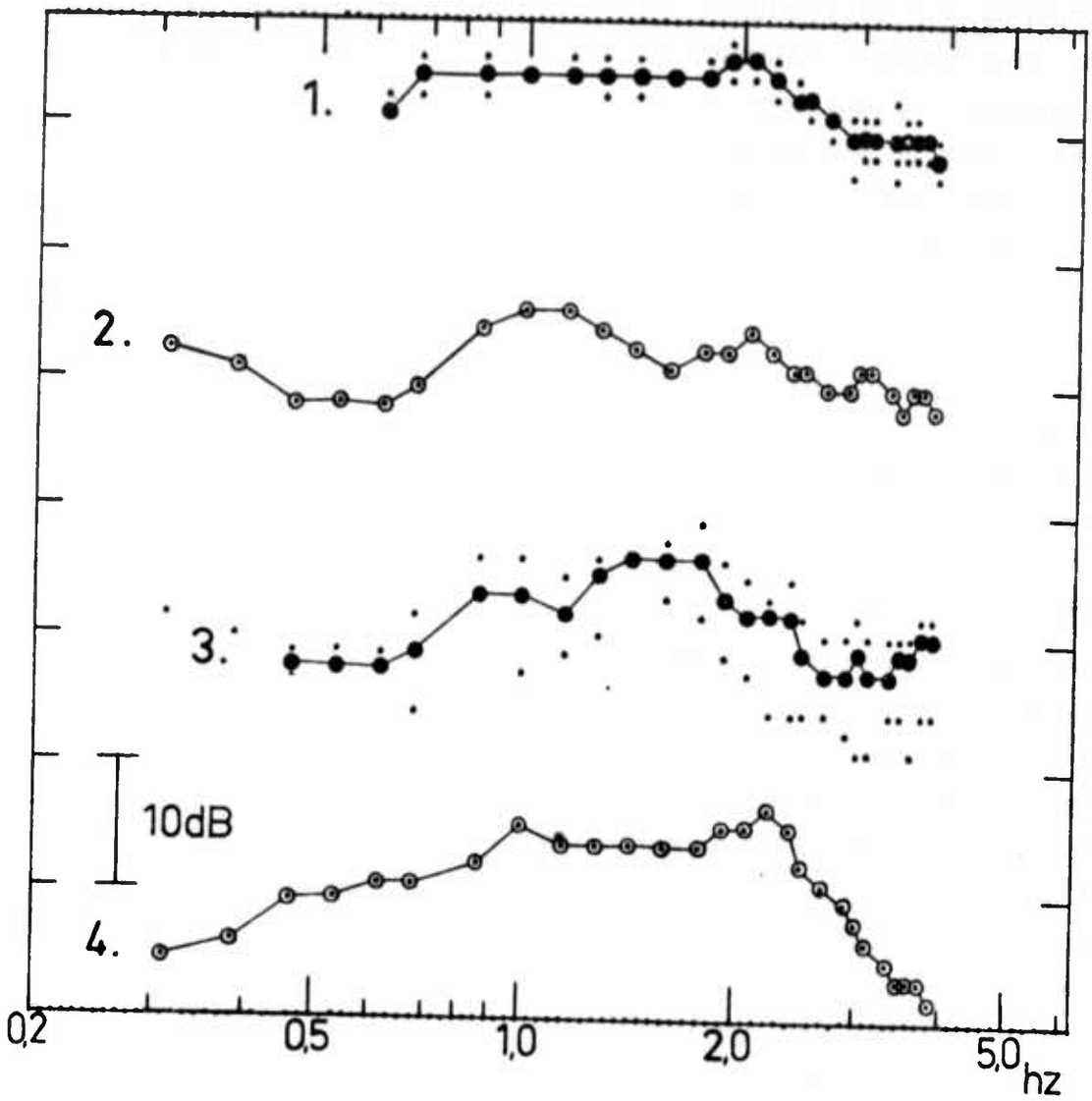

Fig. III.8. Normalized acceleration spectra (asterisks) with averages (circles). (1) The 3 presumed explosions in the event set WESTERN KAZAKH in the magnitude range 3.7 - 3.9 m_b(LASA). (2) A presumed explosion in the same event set with magnitude 6.0 m_b. The WESTERN KAZAKH events lie at an approximate distance of 25 degrees. (3) The 2 events of event set EASTERN CAUCASUS with magnitudes 4.9 and 5.1 and at distance of 30 degrees. (4) The CRIMEA event with magnitude 4.6 and distance 22 degrees.

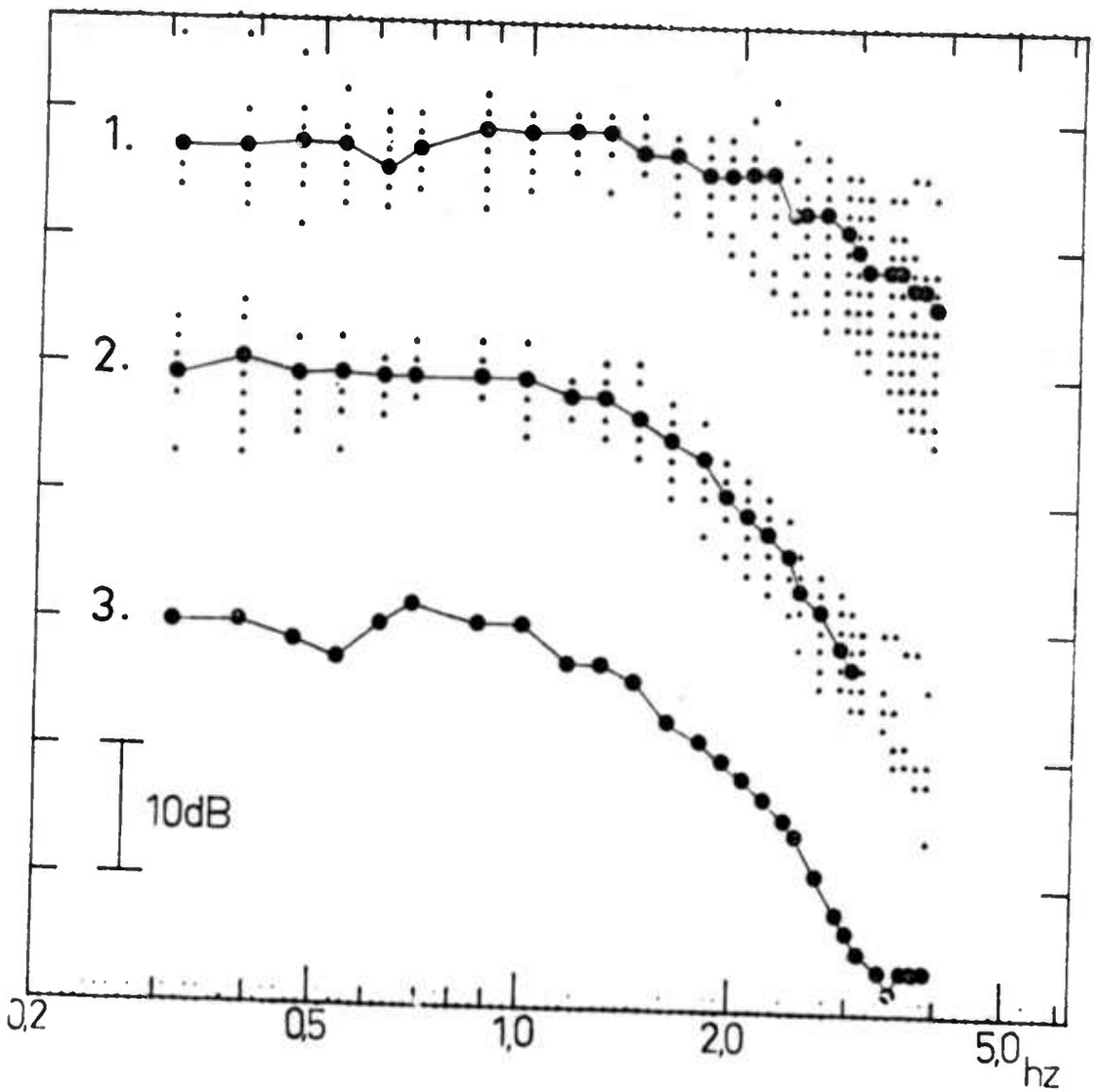

Fig. III.9. Normalized acceleration power spectra (asterisks) with averages (circles). (1) The 16 quakes in the event set GREECE with magnitudes 3.8 - 4.8 m_b and in distance range 20-28 degrees. (2) The 9 quakes in the event set TURKEY in magnitude range 4.1 - 5.0 m_b and in distance range 23-30 degrees. (3) The event in YUGOSLAVIA with magnitude 4.9 and distance 18 degrees.

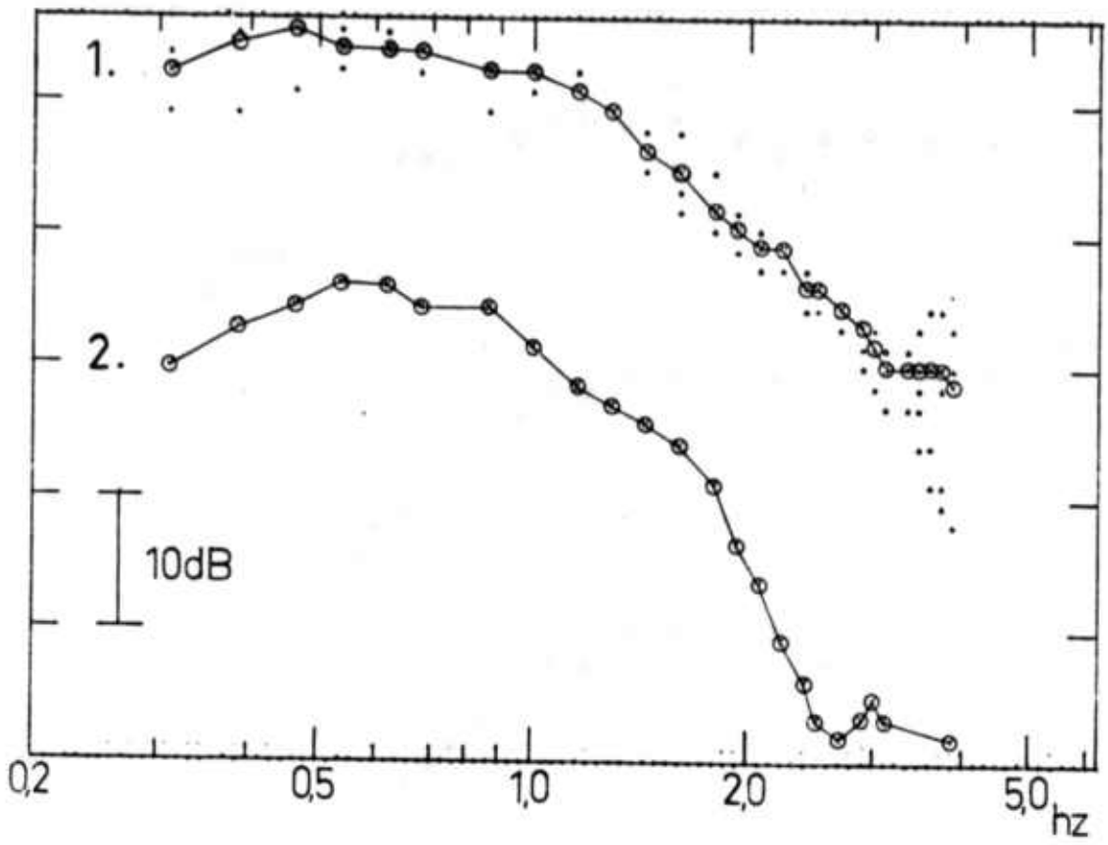

Fig. III.10. Normalized acceleration power spectra (asterisks) with averages (circles). (1) The 4 shocks in event set ITALY in the magnitude range 4.8 - 5.2 and distance range 16-18 degrees. (2) The event in GIBRALTAR with magnitude 4.7 and distance 29 degrees.

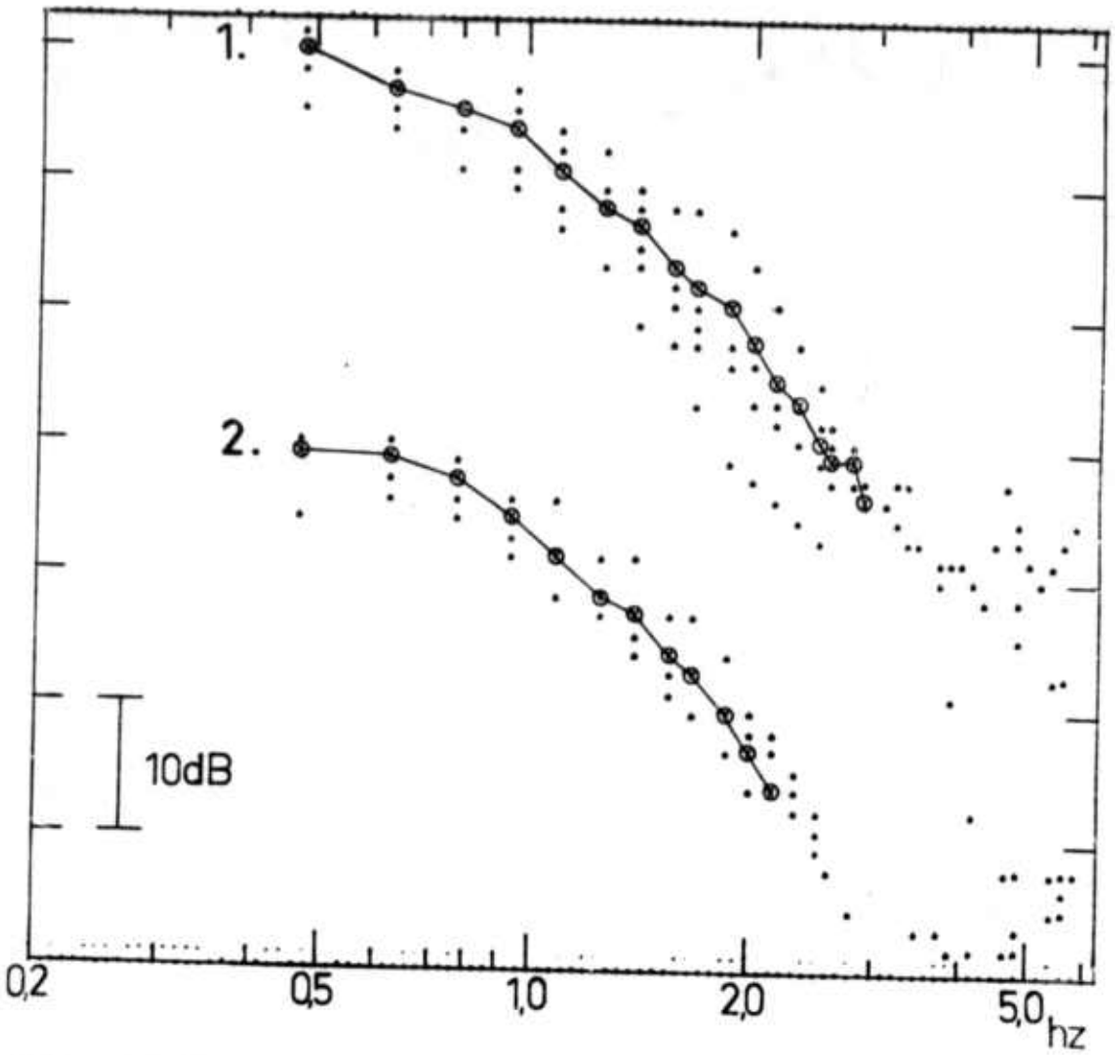

Fig. III.11. Normalized acceleration power spectra (asterisks) with averages (circles). (1) The 6 earthquakes in WESTERN COAST OF NORTH AMERICA event set in magnitude range 4.8-5.6 m_b and in distance range 65-84 degrees. (2) The 5 earthquakes in event set MID-ATLANTIC RIDGE in magnitude range 5.0-5.5 and in distance range 46-61 degrees.

Fig. III.12 (following page). Normalized acceleration power spectra with averages (circles). (1) The 4 events in the event set NEVADA in the magnitude range 4.0-5.0. (2) The 2 events in the same set with magnitudes 5.4 and 5.5. This event set is at distance 75 degrees. (3) 3 events in the event set UTAH/DAKOTA with magnitudes 3.8(NORSAR) - 4.6 m_b. (4) The 6 events in event set GULF OF CALIFORNIA in magnitude range 4.2-5.4 and at distance range 79 degrees. Results above 2-3 Hz are considered unreliable.

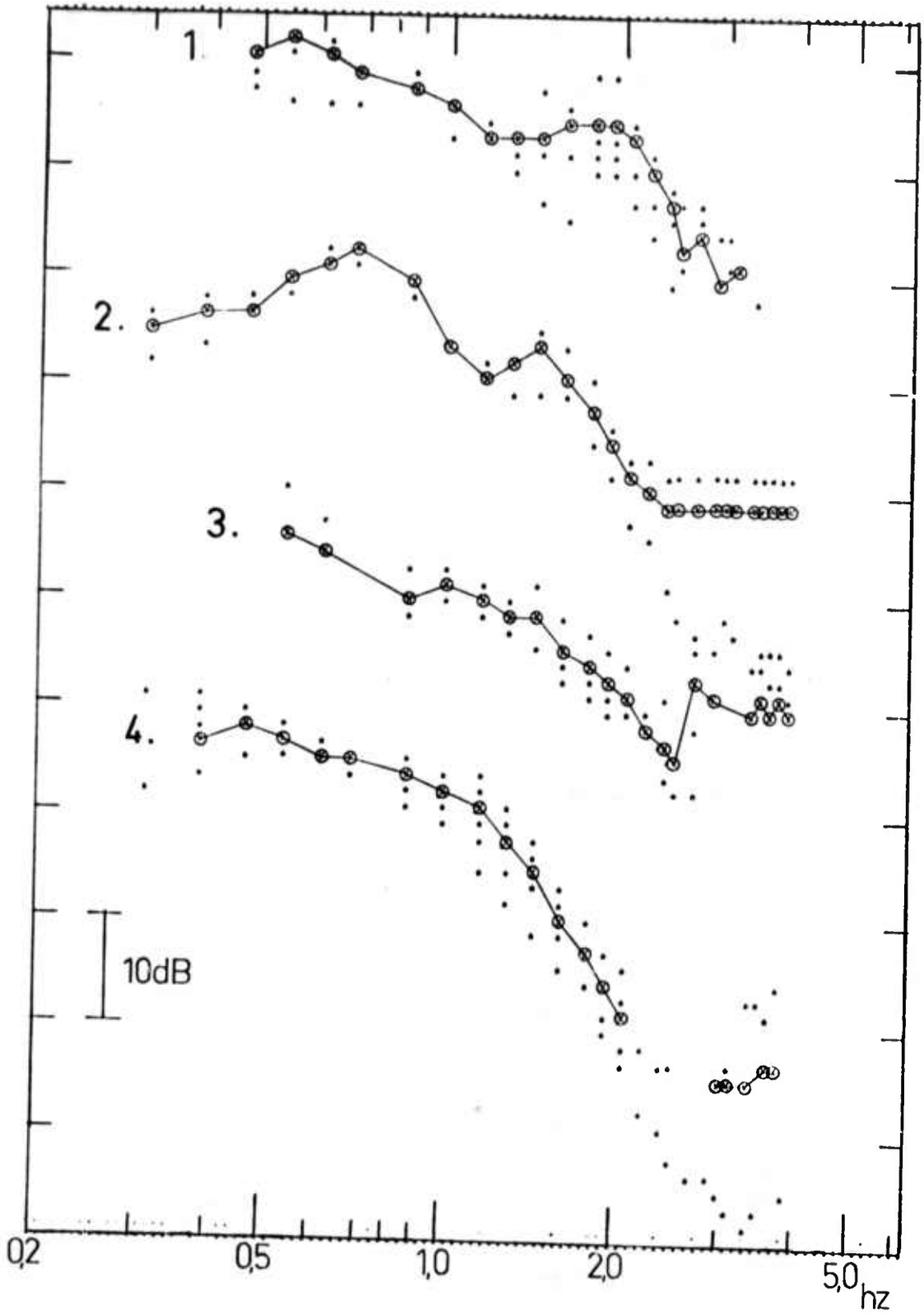

Fig. III.12 (for text see preceding page).

Finally, some ratios between different spectra are displayed. Fig. III.13 shows the ratio of the average spectrum of 6 events in the set WEST COAST OF NORTH AMERICA to the average spectrum of 10 events in the set CENTRAL ASIA (the anomalous event 229 excluded). Over the frequency range 0.2 to 4 Hz the ratio decreases by 20 dB, and the decrease has closely the shape of an exponential function. If the decrease is assumed to be due to a larger attenuation on the path North America - NORSAR than on the path Central Asia - NORSAR, we get for the t^* parameter a difference of $\Delta t^* = 0.279$ between the two paths by fitting the function

$$\exp(\pi f \Delta t^*) \qquad \text{(III.1)}$$

to data. The corresponding curve is plotted to the figure. It approximates the observations with a 0.5 dB r.m.s. scatter. The implied assumption is the similarity of the two average source spectra. All events are within the magnitude range 4.8-6.0. The spectra are smoothed over a bandwidth of 0.62 Hz.

Fig. III.14 shows the ratio of the average of 6 explosion spectra in the set EASTERN KAZAKH to the average of 10 earthquake spectra in the set CENTRAL ASIA. The ratio increases by 20 dB over the frequency range 0.5 to 5 Hz. A simple exponential function which gave an excellent fit to the previous ratio does not fit now, even if we disregard the ripples and consider only the trend of the ratio. The best-fitting exponential function is plotted to the figure. The best fitting function of the form af^{2m} where f is frequency and a, m are constants to be determined is also plotted. For m is obtained the value 1.0. The key question is apparently whether fig. III.14 means that the source spectra of earthquakes and explosions are systematically different up to the frequency 6 Hz, i.e. frequencies much higher than the corner frequency, which for these events with magnitudes above 5.0 is situated at or below 1.0 Hz.

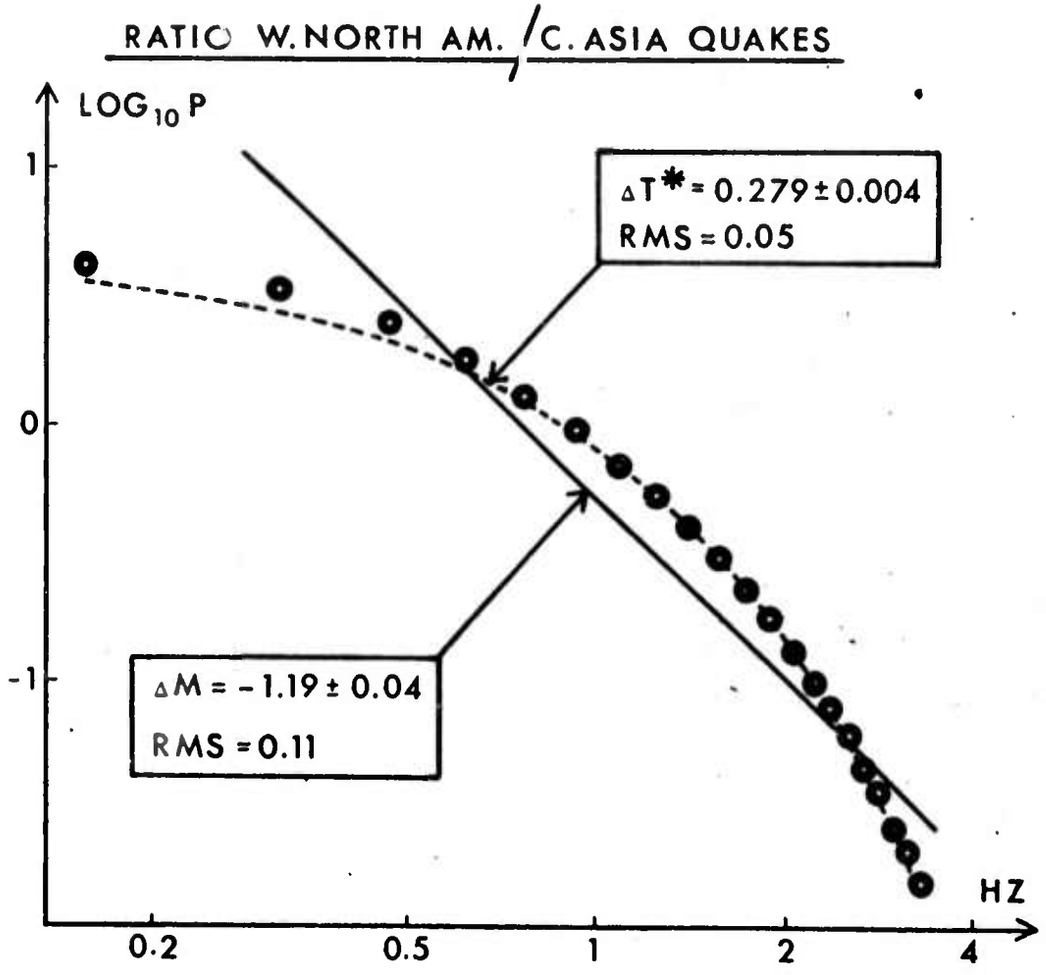

Fig. III.13. Ratio of the average spectrum of earthquakes on west coast of North America to the average spectrum of earthquakes in Central Asia. The broken line describes the best fitting exponential function and the solid line the best fitting power ΔM of frequency.

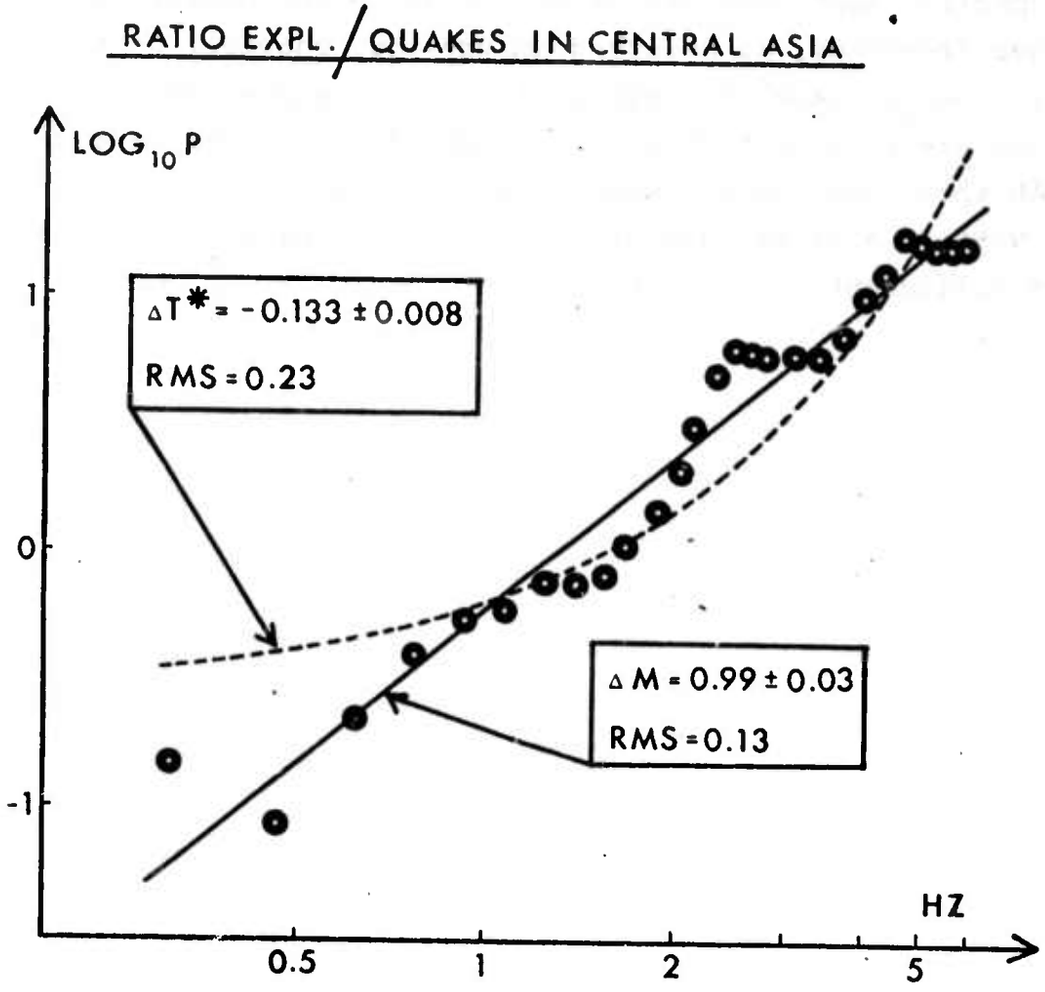

Fig. III.14. Ratio of the average spectrum of Eastern Kazakh explosions to the average spectrum of Central Asian earthquakes. The broken lines describes the best fitting exponential function and the solid line the best fitting power Δ M of frequency.

However, theoretical results suggest the slope of explosion and earthquake spectra to be equal at frequencies sufficiently above the corner frequency[6]. It is concluded that the increase of the ratio at lower frequencies is due to a true difference in the source spectra, most probably caused by different positions of the corner frequency, as observed in previous chapter. On the contrary, the increase of ratio at the high frequencies is explained as due to a less attenuating ray path from the test site to NORSAR than from the seismically active regions of Central Asia to NORSAR. A difference of 0.1 in the t^* values of the ray paths is sufficient.

IV. EXPERIMENT WITH A DISCRIMINANT

The most striking variation among spectra from different regions was found in the relative levels of high and low frequency energy. The underground explosion spectra also differ from earthquake spectra by the relative deficiency of low-frequency energy, when events of equal magnitude are compared. To describe these differences quantitatively, the logarithm of the normalized third moment of signal power about the frequency origin[23] was computed for all spectra. This quantity will be called LTM. Weichert[24] used the third moment of amplitude spectrum for classification, and Anglin[13] added a kind of noise correction to his definition. The definition of LTM is

$$\mathrm{LTM} = \log_{10}\left[\frac{\int_{f_1}^{f_2} (Z(f) - N(f))f^3 df}{\int_{f_1}^{f_2} (Z(f) - N(f))\, df}\right] \qquad (4.1)$$

where Z(f) is an estimate of the power spectrum of the time interval containing the wanted signal, and N(f) is an estimate of the background noise spectrum. Thus the integrals in (4.1) contain no bias due to noise. Because of the variances of estimates Z(f) and N(f) their difference can be positive even when the signal power is nonexistent. In app. 2 the computation of the confidence limits for deciding whether signal power is really present is described. The comparison of the integrated powers to the respective confidence limits indicates whether the LTM measurement is significant.

It turned out that when the low frequency band with largest noise was rejected by defining the frequency limits as f_1 = 0.5 Hz and f_2 = 5 Hz, the LTM values were almost without exception significant for the analyzed events, several of which were on the fringe of detection and location.

In table VI.1 20 event sets are listed, each from a different region. For each region the average value of LTM with standard deviation and coefficient of correlation with event magnitude are shown. Magnitude and distance information are also given. For the sets with significant LTM,m_b correlation parameters of regression line fits to data are given in table VI.2.

Comparing the geographically wide EASTERN ASIA set to the geographically limited SAKHALIN, KURILES and SOUTH OF HONSHU event sets it can be observed that the limited sets have smaller LTM standard deviations and larger LTM,m_b correlation coefficients, and that the average value of LTM differs significantly among these sets. These observations are explained by regional variations of LTM values within the wide EASTERN ASIA set. These variations hide the LTM,m_b correlation in that set.

The regional averages of LTM are plotted to fig. IV.1 as function of distance. It is apparent from the figure that for earthquakes there is no correlation with distance, that the regional differences in LTM are significant and that the strong regional effects destroy the usability of LTM as a classifier, if regional corrections are not included.

A major cause of these regional variations is probably variation of the total anelastic attenuation between the respective ray paths. If the total attenuation parameter t^* differs by 0.1 between two ray paths, this will produce a difference of 0.2 in the LTM value, in average.

Table IV.1. Results of LTM calculations for different regions. Ranges and averages of distance , magnitude m_b and LTM are given. N = number of events, σ is standard deviation of LTM, L largest region dimension in degrees, r is correlation between LTM and magnitude (s means correlation significantly different from zero).

REGION	N	Δ	m_b	LTM range	LTM_{av}	σ	L	r
EASTERN ASIA	15	61-78 67	4.7-6.3 5.3	-0.01/ 0.73	0.338	0.250	30	-0.07
SAKHALIN	20	65-66 65	4.1-5.9 5.0	-0.01/ 0.45	0.215	0.138	1	-0.62 s
KURILES	12	69-69 69	4.3-6.0 4.9	0.34/ 1.02	0.723	0.193	1	-0.69 s
SOUTH OF HONSHU	9	77-77 77	3.9-5.2 4.4	0.09/ 0.57	0.407	0.161	1	-0.36
EASTERN KAZAKH (e)	17	38-38 38	3.8-5.8 5.1	0.63/ 1.14	0.949	0.120	1	0.00
CENTRAL ASIA	13	37-56 45	5.1-6.0 5.4	0.18/ 1.01	0.420	0.222	37	-0.37
WESTERN RUSSIA (e)	6	14-20 17	3.2-5.3 4.7	0.96/ 1.36	1.170	0.206	18	-0.74 s
WESTERN KAZAKH (e)	4	22-24 23	3.7-6.0 4.3	0.72/ 0.88	0.825	0.063	6	0.45
CAUCASUS	2	30,30 30	4.9,5.1 5.0	0.45, 0.95	0.70	-	1	-
CRIMEA	1	- 22	- 4.6	-	0.74	-	-	-
GREECE	20	20-28 24	3.4-5.1 4.4	0.10/ 0.80	0.501	0.231	8	-0.06
TURKEY	9	23-30 26	4.1-5.0 4.5	0.09/ 0.28	0.195	0.073	13	-0.55 s
YUGOSLAVIA	1	- 18	- 4.9	-	0.13	-	-	-
ITALY	6	16-18 17	4.7-5.2 4.9	-0.03/ 0.12	0.077	0.069	3	-
GIBRALTAR	1	- 29	- 4.7	-	-0.08	-	-	-
WEST COAST OF NORTH AMERICA	6	65-83 75	4.8-5.6 5.3	-0.45/-0.08	-0.21	0.158	32	-0.52
MID-ATLANTIC RIDGE	5	45-61 50	4.8-5.2 5.0	-0.49/-0.17	-0.23	0.152	18	-
NEVADA (e)	6	73-73 73	4.0-5.5 4.9	-0.19/ 0.50	0.248	0.228	1	-0.65 s
UTAH/DAKOTA	3	61-70 66	3.7-4.1 3.9	0.05/ 0.60	0.317	0.225	11	-
GULF OF CALIFORNIA	5	79-79 79	4.2-5.4 4.7	-0.10/-0.01	-0.07	0.057	1	-0.56

Table IV.2. Regression line fits to LTM values as function of magnitude for the regions with significant correlation between the two variables. N = number of events, a and b are parameters of the equation LTM = a + bm_b. The r.m.s. scatter around the regression line is also given. (e) stands for presumed explosions.

REGION	N	a	b	r.m.s.
SAKHALIN	20	1.05	-0.169	0.109
KURILES	12	2.08	-0.278	0.139
WESTERN RUSSIA (e)	6	2.15	-0.210	0.139
TURKEY	9	0.869	-0.148	0.061
NEVADA (e)	6	1.613	-0.280	0.173

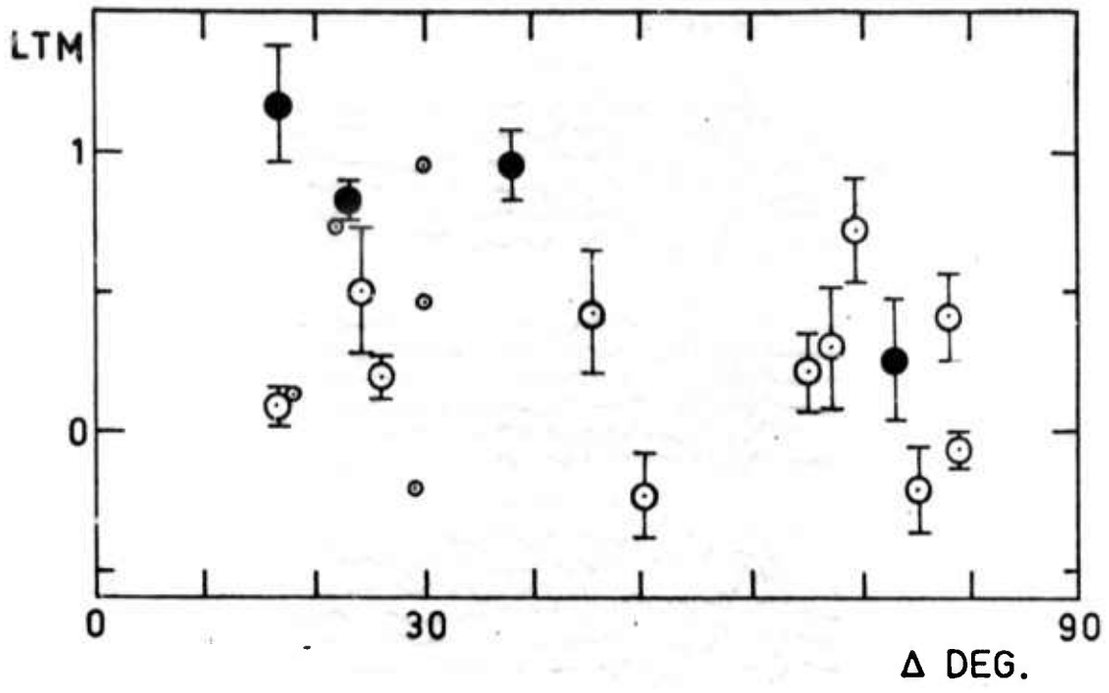

Fig. IV.1. Regional averages of the LTM, a measure of relative amount of high-frequency energy, with standard deviations. Groups of presumed or known underground explosions are plotted with filled circle, earthquakes with open circle. Small circles denote single earthquakes.

The slope of the regression line fitted to the LTM, m_b observations (table IV.2) is typically close to 0.2. Variation of magnitude over the whole observed range 3.8 - 6.3 will then produce an LTM variation of 0.5 units. This is only half of the observed regional variation of LTM (of signal high-frequency contents). E.g. the average LTM values for the event sets MID-ATLANTIC RIDGE and KURILES are -0.23 and 0.72 respectively.

Comparing earthquakes with underground explosions in Eurasia it is observed that explosions have generally higher LTM val-

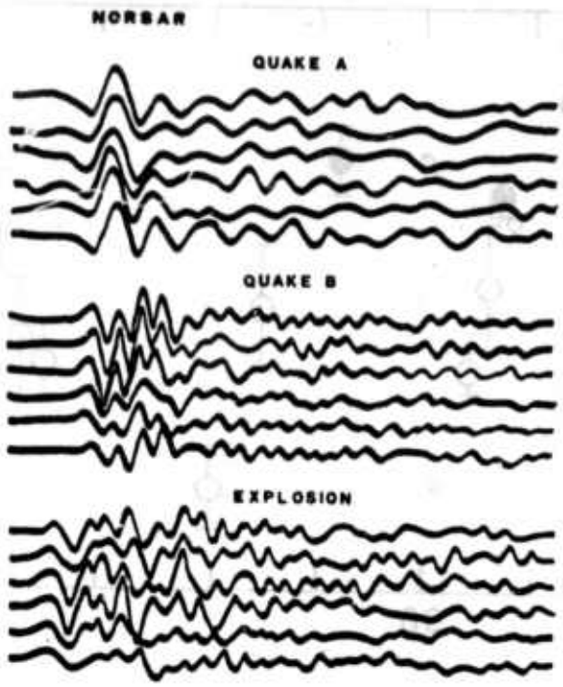

Fig. IV.2. P wave signals recorded at NORSAR subarray 06B from a Central Asian earthquake with normal LTM value (quake A), from the anomalous event 229 in Sinkiang (quake B) and from an explosion in Eastern Kazakh.

ues than earthquakes at comparable distances, as expected. It is difficult to decide whether this is caused by regional variation of wave transmission capability at high frequencies, or whether it is a source effect because no earthquakes have occurred adjacent to explosion sites. There is a variation of LTM values over relatively short distances, e.g. between Italy (low LTM), Greece (high LTM) and Turkey (low LTM).

The event 229 of the CENTRAL ASIA event set has an LTM value of 1.01 which is higher than the mean LTM for explosions in

Eastern Kazakh. Event 229 has been located by NOAA to 42.00°N, 84.58°E, only 20 km from the location of event 108 (41.8°N, 84.5°E) which has a perfectly normal LTM value 0.49. This should exclude the possibility of anomalously low attenuation under event 229. The P wave signals recorded at a subarray of NORSAR from event 229 are compared in fig. IV.2 to signals from another Central Asian earthquake and an E.Kazakh explosion. It is easy to see that the signals of event 229 resemble closely the explosion signals, and that the high value of LTM is really describing the physical reality. The M_s/m_b discriminant suggests this event to be an earthquake (at Nurmijärvi station in Finland M_s = 4.7, m_b(NOAA) = 5.1). The existence of an earthquake having so anomalous P wave spectrum shows that in addition to attenuation variation, the earthquake spectrum can also vary quite unexpectedly.

It is disturbing that the earthquakes closest to the explosions in western and southwestern Russia also have high (explosion-like) LTM values (event sets CRIMEA and CAUCASUS).

When the Nevada explosions are compared to earthquakes in western North America, the astonishing fact appears that earthquakes in the continental U.S. have relatively more high-frequency energy (higher LTM values) than Nevada explosions. If one corrects for the effect of event magnitude by taking the LTM to increase by 0.2 units when magnitude decreases by 1.0 units, as suggested above, the ranges of the LTM values for the two data sets become equal. The earthquakes in the Gulf of California and at the west coast of North America behave well giving lower LTM values than Nevada explosions, in average.

Western North America is a tectonically complex region. Lateral variation in body wave transmission capability have been reported in terms of P wave magnitude anomalies[25,26] and of anelastic body wave attenuation under seismic stations[27]. In

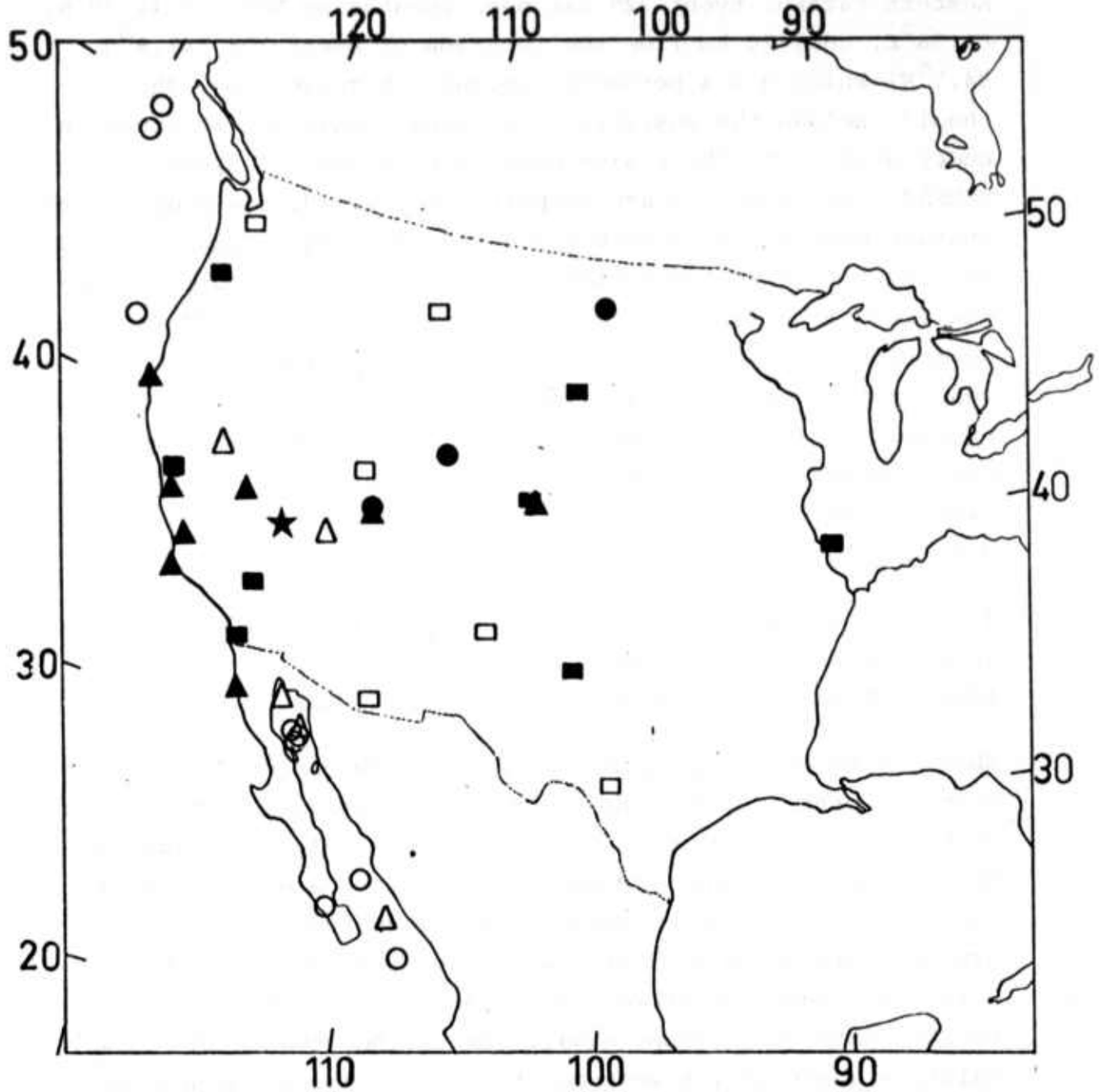

Fig. IV.3. Observations on P wave attenuation in the western U.S.. Attenuation above average is denoted by open symbols, attenuation less than average by filled symbols. Squares mark the stations where attenuation of long period body waves was studied[27], triangles mark earthquakes used in P wave magnitude anomaly studies[25,26] and circles mark the earthquakes for which the LTM values were computed in this study. The asterisk denotes the Nevada test site.

fig. IV.3 those observations are shown together with observations made in this study, plotted on a map of the western U.S.. Observations indicating poor P wave transmission are shown with open symbols, good transmission is indicated by filled symbols. A region with poor P wave transmission runs in north-south direction, comprising the Basin and Range region and the region around and east of the Gulf of California. The Nevada test site is situated near the border of this region. As poor body wave transmission capability attenuates most the high-frequency waves, it is apparent why the earthquakes in eastern Utah and Dakota tend to have high LTM values and the Gulf of California shocks have low values. The position of the Nevada test site is intermediate to these, and there is again the difficulty of telling how great actually is the source effect on the LTM values. Manchee[28] observed spectra of Nevada and the Gulf of California events and concluded that a short-period spectral discriminant can be used to separate explosions in Nevada from the Gulf of California shocks. Apart from any improvement stemming from his particular definition of a short-period discriminant, it seems that a part of the separation comes from the strong attenuation of high frequencies at the Gulf of California region.

A correlation of LTM variation with tectonics appears when it is observed that high values of LTM are associated with regions where intermediate or deep earthquakes occur in addition to shallow shocks. Examples of this are the event sets GREECE (average LTM 0.50), KURILES (0.72), SOUTH OF HONSHU (0.41). Low values of LTM are associated with seismically active regions where only shallow quakes occur. Examples are TURKEY (0.19), (northern) ITALY (0.08), MID-ATLANTIC RIDGE (-0.23), WEST COAST OF NORTH AMERICA (-0.21), and also SAKHALIN (0.21).

This correlation can be explained as caused by increased rigidity of the upper mantle in regions with deep shocks. The rigid

mantle can produce tensions necessary for earthquakes, and does not attenuate strongly the high-frequency waves. From the point of view of plate tectonics, one could say that the P waves propagate along the cold and rigid plates through the upper mantle. In case of weakly seismic regions or boundary zones between seismic and aseismic regions our present knowledge is not sufficient to predict the expected range of LTM values. If the upper mantle has a very small attenuation (high rigidity) under the aseismic regions where the explosions in Eurasia occur, the LTM (and TMF) difference between these explosions and the earthquakes of the seismic belt could be mainly due to a difference of attenuation in the upper mantle.

In figures IV.4 (a-c) LTM values of the earthquakes closest to the explosion sites are plotted as a function of distance from the explosion site. The LTM values are corrected for magnitude by using a $d(LTM)/d(m_b)$ of 0.2 and reducing the LTM values to a $m_b = 5.0$ earthquake. The figures would be essentially similar without correction. When the earthquake-explosion site distance decreases, the separation between earthquake and explosion LTM values also decreases. It seems that for an earthquake occurring close to the explosion site, or vice versa, classification using LTM measure would be very uncertain. Comparison with measurements made at Hagfors station[29,30] indicate that no improvement is achieved by use of the original TMF discriminant.

It is concluded that the LTM discriminant is unsuitable for separating earthquakes and explosions because its separation distance is small compared with effects of regional attenuation variations. Because the TMF discriminant[24] gives results which are (after taking logarithm of TMF) linearly correlated with the LTM measure (for a sample of 25 events[30] the correlation coefficient was 0.88 between the two measures) it is expected that the same difficulties are met when using that discriminant.

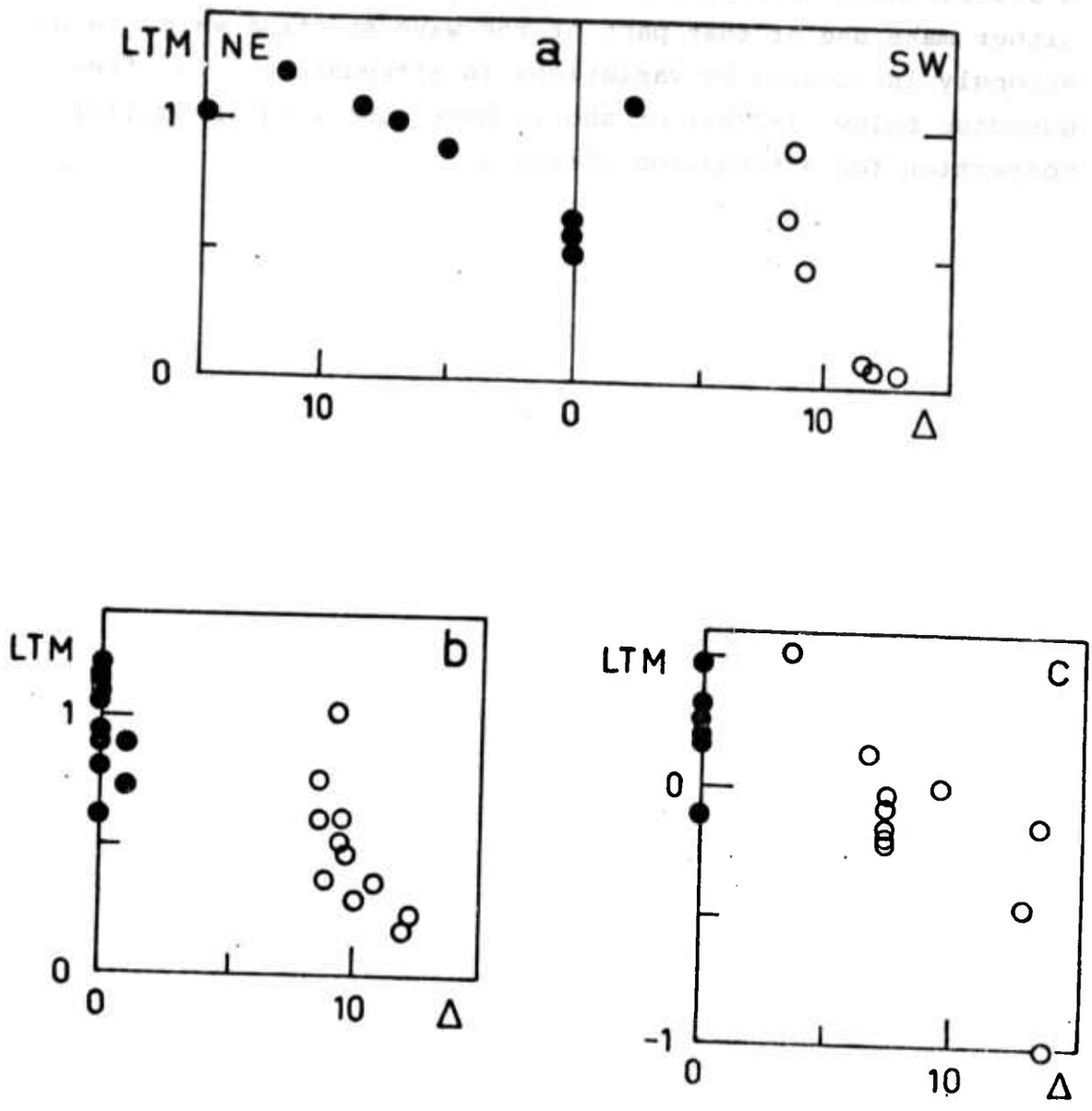

Fig. IV.4. LTM values of events plotted as a function of distance from explosion sites. The values are corrected for effect of magnitude. In (a) distances are computed from 50 N 47 E Western Kazakh presumed test site. Events in NE and SW quadrants are computed to left and right from zero distance, respectively. In (b) distances are computed from 50.0 N,77.6 E (Eastern Kazakh test site). In (c) distances are computed from 37.1 N, 116.1 W (Nevada test site). Presumed explosions and earthquakes are plotted with filled and open symbols,respectively.

A discriminant employing short period P wave spectrum should either make use of that part of the wave spectrum which is not strongly influenced by variations in attenuation (i.e. frequencies below 1-2 Hz) or should have some kind of built-in correction for attenuation effects.

V. SUMMARY AND CONCLUSIONS

A large seismic array was used for estimation of the spectra of P wave signals with proper corrections made for the influence of noise and instrument response. The spectra computed for earthquakes follow in principle the predictions from analytical models of the seismic source. The properties flat power spectrum at low frequencies, at high frequencies an average power decrease proportional to ω^{-n} where probably n = 2 and between these trends a corner frequency which is associated with the source size agree well with the spectra presented in chapter II. According to Randall[31] both the dislocation and stress-relaxation models exhibit these features.

A five-fold variation of corner frequency (0.2 - 1.0 Hz) for shocks of magnitude 5.6 is observed. If the event 229 in Sinkiang with anomalously strong high-frequency waves is interpreted as having a very high corner frequency of 4 Hz, the range of variation is even larger for events within a rather narrow magnitude range. With an inverse proportionality between source size and corner frequency[5,31] this would imply a strong variation in earthquake fault lenghts.

The explosion-generated P wave signal spectra agree in principle with analytical models of Mueller and Murphy, and of Haskell (reviewed and revised by Seggern and Blandford[6]). The spectra predicted by these models also have a corner frequency and an ω^{-2} fall-off at high frequencies. The main difference from the predicted earthquake spectrum is at frequencies below the corner frequency, where the explosion power may decrease towards zero frequency, so that a maximum appears at the corner frequency[32]. In most cases the explosion P wave signals did not have measurable power at frequencies below the corner frequency due

to noise interference. This was a difficulty in the analysis of the explosion spectra, together with the fact that the spectra at the high corner frequencies of explosions began to be distorted by the anelastic attenuation.

When the corner frequencies were estimated visually from the explosion spectra, allowing for a slight effect of attenuation, they were observed to lie at roughly three times higher frequencies than the corner frequencies of earthquakes with similar magnitudes. This causes the low-frequency levels of the explosion spectra to remain below those of the earthquake spectra. The difference may be heightened by a decrease of explosion power from corner frequency towards zero frequency. At frequency 0.3 Hz the spectral power of Eastern Kazakh explosions in magnitude range 5.2 - 5.8 is systematically 20 dB less than the spectral power of earthquakes in Central Asia with similar magnitudes. It is impossible to say how this ratio develops at even lower frequencies because the earth noisecovers there the explosion signal.

Up to here we have discussed a frequency range where the effect of anelastic attenuation during wave transmission is of minor importance. But in the comparison of spectra at frequencies above 2 Hz, the attenuation of high frequencies becomes a dominant factor. The attenuation variation within the Earth probably causes the systematic regional variation in the relative levels of high and low frequency energy noted when frequencies up to 4 or 6 Hz are observed. This conclusion is supported by the following arguments: (a) In comparing the spectra from events of same type and magnitude but at different regions, the shape of the difference in spectra could well be explained by a different amount of frequency-independent Q type attenuation on the respective propagation paths. (b) Spectra rich in high frequency energy were observed from regions where in addition to shallow seismic activity also deeper shocks occur. Deep shocks are an indication of in-

creased mantle rigidity which is expected to be coupled with smaller anelastic attenuation of seismic waves.

The possibility of systematic variation in the earthquake source spectra between the different regions should not be neglected, though reasons for such a variation are not apparent. The variation of the relative high-frequency contents within source regions very small in extent should reflect true variation in the source spectra. This was studied using three event groups in Eastern Asia, each less than a degree wide. The high-frequency contents of each event was indicated by a measure termed LTM. After an empirical magnitude correction was made to the LTM values, their distribution around the event group mean value resembled closely a normal distribution. But the case is not always this simple, quite unexpectedly one of the earthquakes (229) in Central Asia displayed an LTM value and spectral shape greatly differing from other events in the Central Asian population. It seems that in addition to a 'normal' source variation of the relative high-frequency contents (LTM value) within an event group, outliers may also appear.

The LTM measure is a logarithm of the noise-corrected normalized third moment of power in respect to frequency origin. It is thus a modification of the TMF discriminant[24], the motive for a new definition is to achieve a sound noise correction. Values of LTM and log(TMF) are linearly correlated, so the conclusions made for LTM apply also to TMF.

In comparing values of LTM for explosion and earthquake signals it was observed that the regional variations of both earthquake and explosion LTM values are so large that general comparison is impossible. It was not possible to find really comparable earthquake and explosion transmission paths. It seems that the events should not be separated by more than 1-2 degrees, for unambiguous comparison[30]. The earthquakes closest to explosion

sites also had the most explosion-like (high) LTM values.

We can roughly divide the present event source regions to three types: one with only shallow seismicity (low LTM values of earthquakes), a second with both shallow and intermediate or deep seismicity (high LTM values of earthquakes) and as a third type aseismic platforms (very high LTM values for explosions). In the almost complete absence of absolute information on anelastic attenuation, the possibility cannot be denied that the LTM value differences also between explosions and earthquakes in Eurasia are mainly due to transmission path differences, caused by a (hypothetical) very low wave attenuation under a stable platform. At least it seems apparent that if earthquakes in high-attenuation regions of only shallow seismicity are compared to explosions on stable platforms for assessment of the classification capability of classifiers like TMF, far too positive results are obtained.

It is concluded that event classifiers using only P waves can best be designed by using in some suitable manner the one difference between earthquakes and explosions well documented both by theory and observation, the difference in the respective corner frequencies of spectra, maybe together with the (less well documented) behaviour of the spectra at frequencies below the corner frequency. It will be necessary to take into account the predicted variation of corner frequency with event magnitude. Future work will be directed along these lines.

APPENDIX 1

SIGNAL-TO-NOISE RATIOS, BEAM LOSSES AND STABILITIES

Estimates on P wave signal-to-noise ratio (SNR) and beam loss (due to incoherency of signals across the array) as functions of frequency have been made for 6 explosions in E.Kazakh and 9 earthquakes in Central Asia. The results reviewed here have been published[16]. Events are in the magnitude range 5.0-6.0 m_b. Power spectra of P waves recorded by all single sensors of NORSAR were computed and averaged over the sensors, for each event. The average signal spectra were then noise-corrected, smoothed, normalized and averaged within each group of events. The average earthquake and explosion spectra were then compared to an average of noise spectra measured at 15 random dates and times of year. Table 1 summarizes the SNR results. The column marked f_{max} gives the frequency of maximum SNR and columns f_{12} give frequencies at which SNR is 12 dB down from the maximum

Table 1. Summary of SNR measurements for Central Asia

event type	f_{12}	f_{max}	f_{12}
earthquakes	0.7 Hz	2.0 Hz	4.5 Hz
explosions	1.4 Hz	2.6 Hz	5.2 Hz

The beam losses were also computed separately for explosions and earthquakes. For each event, the signal power spectrum of the array beam was compared to the average signal power spectrum of the single sensors. Their ratio is the beam loss. The losses were averaged within each group of events. The av-

erage of the subarray beam spectra was similarly compared to the average of the single sensor signal spectra for each event, and the subarray beam losses again averaged within each event group. The results are shown in figs A1.1 and A1.2. The figures show that the signal losses approach the suppression of a random signal at the frequency 5 Hz (random signal is expected to be suppressed by 21 dB in the array beam and 7.8 dB in a subarray beam). The length of time intervals taken for spectral analysis was 6.4 sec.

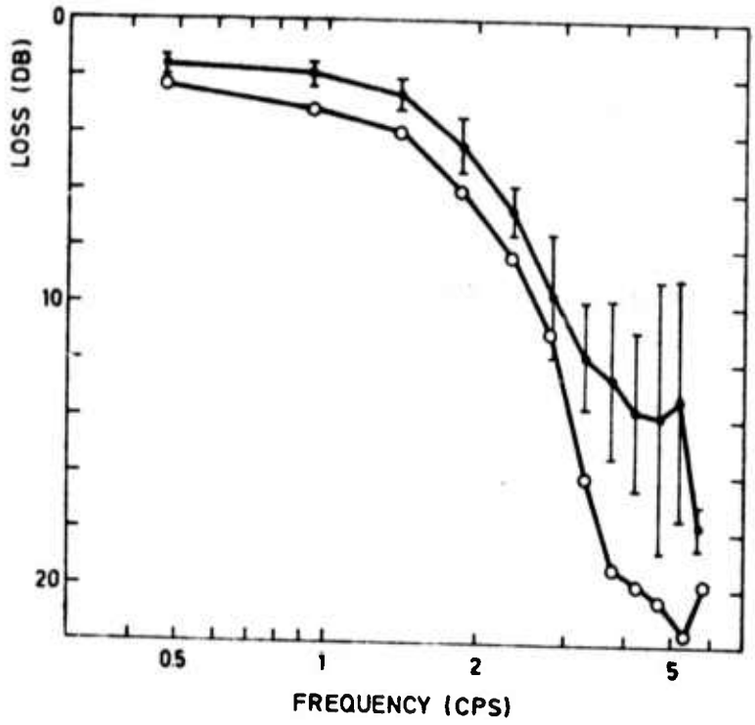

Fig. A1.1. The loss of signal power in array beamforming relative to the average signal power at the single sensor level, as a function of frequency. The losses are averaged over several events. They are computed separately for Central Asian earthquakes (closed circles with standard deviations) and explosions (open circles).

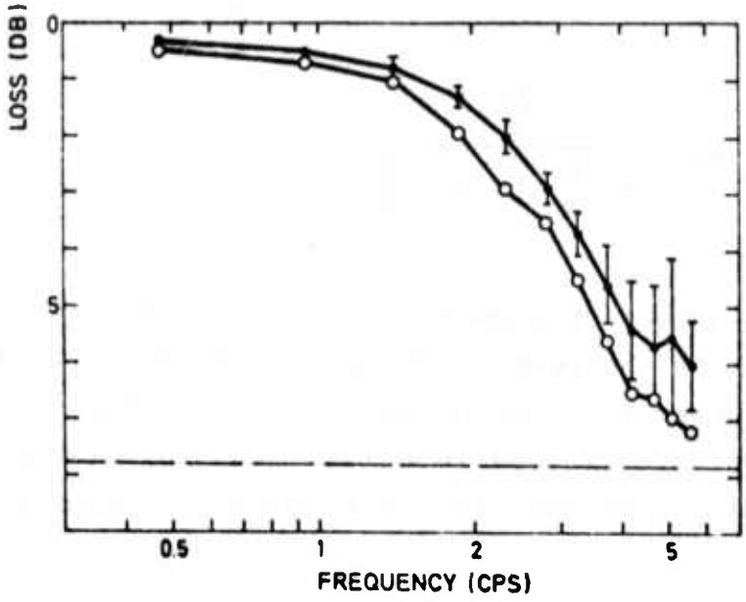

Fig. A1.2. The loss of signal power in subarray beamforming relative to the average signal power at the single sensor level, as a function of frequency. The losses are averaged over all subarrays and several events. They are computed separately for Central Asian earthquakes (closed circles with standard deviations) and explosions (open circles).

The observed SNR and beam loss were used in the estimation of stabilities of spectra computed by different forms of array processing. The following equations given by Lacoss and Kuster[15] give the stabilities s_p and s_b of the single sensor average signal spectrum and beam signal spectrum, respectively.

$$s_p = \frac{Kr^2}{4\ (r + (1 + \frac{K}{L}))}$$

$$s_b = \frac{(\frac{Kr}{g})^2}{4\ (\frac{Kr}{g} + (1 + \frac{1}{L}))}$$

where K is the number of sensors used in averaging the signal spectra or forming the beam, r is twice the ratio of single sensor signal power to noise power, g^{-1} is the beam loss and L is the number of blocks used in estimating the noise power spectrum. The stability of the average of subarray beams is

$$s_a = \frac{N(\frac{Mr}{e})^2}{4\ (\frac{Mr}{e} + (1 + \frac{1}{L}))}$$

where N is the number of subarrays, M is the number of sensors in each subarray, e is the average subarray beam loss and r and L are as above.

The beam loss and SNR observations for Central Asian earthquakes were put to the equations above, the SNR being scaled suitable for a 4.8 magnitude shock. The resulting stabilities as functions of frequency are shown in fig. A1.3. It is concluded that the average of subarray beams has a good stability at a wide range of frequencies, processing does not use an excessive about of computing time and the observed spectrum is not distorted by more than 6-7 dB in the worst case. It is

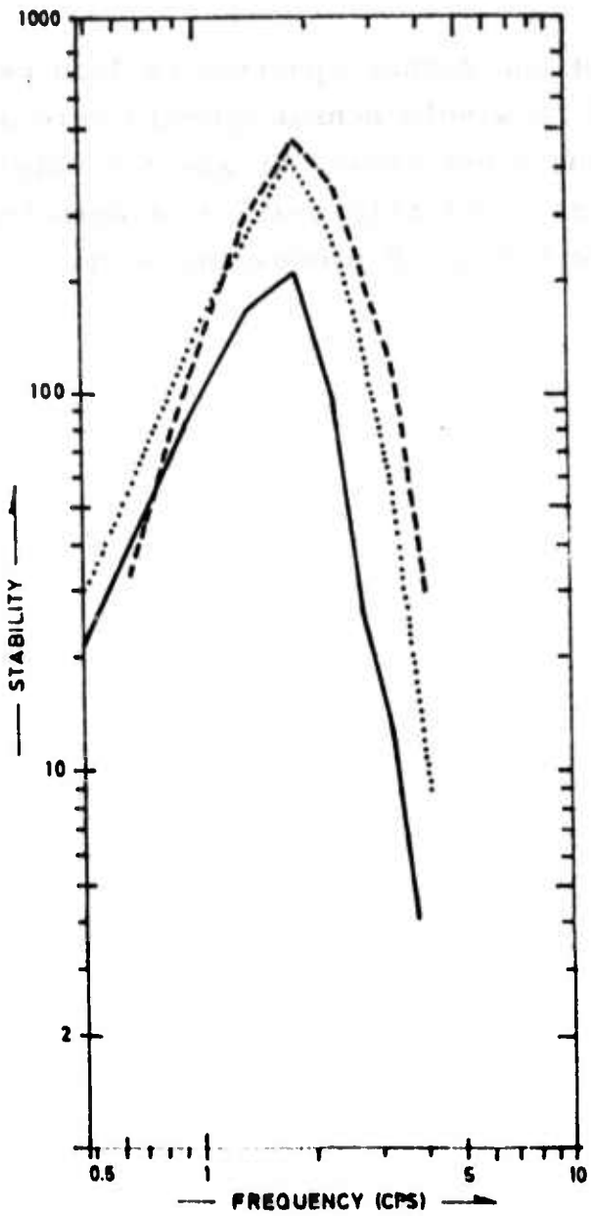

Fig. A1.3. Stabilities for different forms of precessing array data, computed from loss and SNR observations for the earthquakes in Central Asia, scaled to m_b 4.8. Continuous line is beamforming, broken line is spectraforming and dotted line is spectraforming of subarray beams.

selected as the short period array processing method used in this study.

The stabilities of the signal spectrum on long period beam and of the average of LP single sensor spectra were also computed using the equations given above. It was concluded that because the LP beam loss is apparently small (not more than a few dB) beamforming is the better LP processing method at all signal-to-noise ratios.

APPENDIX 2

NOISE-CORRECTION, NORMALIZATION AND AVERAGING OF SPECTRA

Z(f) is taken to be the power spectrum of a section of recording which is supposed to contain a transient signal and noise (f = frequency). The power spectrum of the pure signal is assumed to be $|S(f)|^2$. Y(f) is the power spectrum of a section of the same recording, containing only noise. The noise is assumed to be a stationary random Gaussian process with zero mean and uncorrelated with the signal. The noise power Y(f) has at each frequency, by definition, a probability density distribution identical to a multiple of the χ^2 distribution with two degrees of freedom[22]. The recordings from which these sections are taken may be from a single sensor, a subarray beam or the array beam.

An estimate of signal power is made by subtraction

$$P(f) = Z(f) - Y(f) \tag{1}$$

The expected value of P is[15]

$$E(P) = |S|^2 \tag{2}$$

where the implicit dependence on frequency is not written, for brevity.

If $|S|^2 = 0$ then E(P) is also zero and two estimates of noise power are being subtracted from each other. Because the estimates are less than perfect, values of P larger than zero can occur. We want to be on guard against the situation where such occurrence is taken to indicate signal power, while true signal power is zero or practically zero.

The stability of the estimates of Z and Y can be improved by ensemble averaging and frequency smoothing. Considering ensemble averaging, if there are available N parallel channels recording the same signal but different realizations of noise, as is the case with an array station, the signal and noise section stabilities can be improved by averaging over these.

Because several noise sections at different times can be analyzed from each channel, the number M of noise sections can be larger than N. Even though the noise is here assumed to be roughly an ergodic process, the ergodicity is in all probability so incomplete that one does best by including all channels to noise averaging in equal proportions.

The averages are

$$Z = \frac{1}{N} \sum_{n=1}^{N} Z_n \qquad Y = \frac{1}{M} \sum_{m=1}^{M} Y_m \tag{3}$$

When $|S|^2 = 0$ the probability density distributions for both are multiples of χ^2 distributions with 2N and 2M degrees of freedom.

The variance of P given $|S|^2 = 0$, when P is estimated as $P = Z-Y$, is the sum of the variances of Z and Y. These can be deduced from their χ^2 density distributions. We get for the variance of P

$$\sigma^2(P) = \left(\frac{1}{N} + \frac{1}{M} \right) \left[E(Y) \right]^2 \tag{4}$$

When $N,M \gg 1$ the probability density distributions of the quantities Z, Y and P approach closely normal distributions. Then it is easy to define confidence limits for P given $|S|^2 = 0$. The 99% confidence limit has been used, or if

$$P > 2.58 \left(\frac{1}{N} + \frac{1}{M} \right)^{\frac{1}{2}} Y \qquad (5)$$

we were 99% confident in making the right decision when it was concluded that signal power is present. When P did not fulfil inequality (5), the power estimate at that frequency was rejected.

When the array beam is used, N = 1 by necessity. To decrease the variance of P, M can be increased either by analyzing several successive noise sections of the beam recording, or by analyzing the constituents of the array beam, the single sensor or subarray beam recordings, and then simulating the noise reduction in beamforming by dividing their average power by the number of sensors or subarray beams used in forming the array beam, respectively.

When estimating the spectra from recordings of long period sensors presented in this paper, the latter way was used. In addition to the signal section spectrum from the long period array beam, noise spectra from M single sensor recordings were computed, averaged and divided by N. Usually M was 10, the sensors of the outermost sensor ring of NORSAR were used to avoid any local noise anomalies.

When N is as small as 1 the probability density distribution of Z deviates from the normal distribution. In computing the long period spectra with N = 1, this deviation was neglected and ineq. (5) used. Usually some frequency smoothing was made and in the summing of the different frequency components the central limit theorem was shaping the distribution of Z towards normal distribution.

Spectra from both long and short period sensors were smoothed

over frequency. The purpose was twofold: the most rapid variations of the spectra were not needed at this level of the analysis of data, also smoothing increases the stability of the noise estimates making possible to dig deeper to noise for signal.

The variances of power P given $|S|^2 = 0$ at frequencies $f_1, f_2 \ldots f_k$ are given by eq.(4). The variance of the average power P_A over K frequencies is then

$$\sigma^2(P_A) = \left(\frac{1}{N} + \frac{1}{M} \right) \frac{1}{K^2} \sum_{k=1}^{K} Y^2(f_k) \qquad (6)$$

If all $Y(f_k)$ are equal, the variance of the average power is decreased by a factor of K relative to the individual variances. Usually this is not the case, however, the variance always decreases in smoothing, with a corresponding narrowing of the confidence limits of P_A. The confidence limits of P_A can easily be estimated because of its normal probability distribution.

To average spectra from several, say J, events each spectrum is first normalized. For an event j the normalizing factor is computed as

$$F_j = \int_0^\infty Z_j(f) - Y_j(f)\, df$$

Power of noise and signal spectra averaged over events is

$$\text{ave}\left[Z_j(f)\right] = \frac{1}{J} \sum_{j=1}^{J} \frac{Z_j(f)}{F_j}$$

$$\text{ave}\left[Y_j(f)\right] = \frac{1}{J} \sum_{j=1}^{J} \frac{Y_j(f)}{F_j}$$

The average pure signal power P_A is then

$$P_A = \text{ave}(Z_j(f)) - \text{ave}(Y_j(f))$$

with variance

$$\sigma_A^2 = \left(\frac{1}{N} + \frac{1}{M} \right) \frac{1}{K^2} \frac{1}{J^2} \sum_{j=1}^{J} \left(\frac{Y_j(f)}{F_j} \right)^2$$

where the individual signal and noise spectra are assumed to come from ensemble averaging over N and M channels and to be smoothed over K frequency components. If the individual spectra resemble each other the stability is increased in averaging over events.

Eq. (4.1) for computation of the third moment of power has integrals over power in denominator and nominator. The variance σ^2 of the denominator integral (written as sum over K frequency components) is

$$\sigma^2 = \left(\frac{1}{N} + \frac{1}{M} \right) \sum_{k=1}^{K} f_k^3 \, Y(f_k)^2$$

The variance of the integral in nominator is similar save the absence of factor f_k^3. From the central limit theorem follows that the probability density distributions of the two integrals are normal, and confidence limits for both can thus easily be computed from the standard deviations.

APPENDIX 3

In the following table the events discussed in this report are listed. They are grouped geographically, the groups containing up to 23 events. Events in Asia are listed first, then events in Europe and then events in North America. Some large events are separately added to the end of the list.

CODE	EPX	Y	M	D	H	M	S	LAT		LONG		D	MB	REGION	SOURCE	LTM
---	EVENT SET - EASTERN ASIA															
201		71	9	5	18	35	25	46.5	N	141.2	E	9	6.3	SAKHALIN ISLANDS	NOAA	0.079
202		71	9	5	19	33	47	46.4	N	141.2	E	15	5.5	SAKHALIN ISLAND	NOAA	-0.010
203		71	9	5	20	37	1	46.7	N	141.2	E	N	5.0	SAKHALIN ISLAND	NOAA	0.438
204		71	9	6	2	59	39	46.7	N	141.2	E	N	5.4	SAKHALIN ISLAND	NOAA	0.240
205		71	9	9	23	1	7	44.4	N	150.9	E	7	6.0	KURIL ISLANDS REGION	NOAA	0.583
206		71	12	15	9	22	36	55.9	N	163.7	E	N	5.2	EAST COAST OF KAMCHATKA	NOAA	0.009
207		71	12	15	11	10	48	55.7	N	163.9	E	N	4.7	EAST COAST OF KAMCHATKA	NOAA	0.201
208		71	12	15	12	1	46	55.7	N	164.1	E	N	5.1	KOMADORSKY ISLANDS REGION	NOAA	0.285
209		71	12	15	13	7	43	55.7	N	164.1	E	32	5.3	KOMADORSKY ISLANDS REGION	NOAA	0.000
211		72	5	23	18	3	22	33.5	N	142.3	E	19	5.1	EAST COAST OF HONSHU	NOAA	0.376
212		72	6	15	15	21	20	42.4	N	143.0	E	76	5.5	HOKKAIDO JAPAN REGION	NOAA	0.464
213		72	6	19	1	2	54	52.2	N	175.0	E	53	5.3	RAT ISLANDS ALEUTIAN IS.	NOAA	0.727
214		72	6	19	1	43	48	54.4	N	168.6	E	N	5.0	KOMADORSKY ISLANDS REGION	NOAA	0.290
215		72	6	28	1	50	43	37.4	N	141.3	E	70	5.4	NEAR EAST COAST OF HONSHU	NOAA	0.714
228		72	4	17	10	35	45	25.6	N	95.4	E	108	5.0	BURMA-INDIA BORDER REGION	NOAA	0.680
---	EVENT SET - SAKHALIN															
S01	93710	71	9	5	19	59	41	46.5	N	141.0	E	N	4.7	SAKHALIN	NOAA	0.198
S02	94050	71	9	5	20	42	58	46.6	N	141.0	E	N	4.4	SAKHALIN	NOAA	0.083
S03	94190	71	9	5	21	13	57	46.5	N	140.9	E	N	4.6	SAKHALIN	NOAA	0.400
S04	95850	71	9	6	4	21	43	46.9	N	141.4	E	26	4.8	SAKHALIN	NOAA	0.420
S05	96080	71	9	6	5	33	5	46.7	N	141.2	E	N	4.5	SAKHALIN	NOAA	0.220
S06	96280	71	9	6	7	43	41	46.7	N	141.0	E	N	4.2	SAKHALIN	NOAA	0.270
S07	96500	71	9	6	10	43	32	46.4	N	141.4	E	41	4.7	SAKHALIN	NOAA	0.280
S08	4980	71	9	8	12	58	59	46.2	N	141.0	E	N	4.9	SAKHALIN	NOAA	0.440
S09	5280	71	9	8	15	2	14	46.6	N	141.1	E	N	4.7	SAKHALIN	NOAA	0.310
S10	6650	71	9	8	20	45	1	46.5	N	141.0	E	N	4.1	SAKHALIN	NOAA	0.450
S11	93530	71	9	5	19	33	47	46.4	N	141.2	E	15	5.5	SAKHALIN	NOAA	-0.010
S12	93970	71	9	5	20	37	0	46.7	N	141.2	E	N	5.0	SAKHALIN	NOAA	0.114
S13	95660	71	9	6	2	50	39	45.1	N	141.8	E		5.4	SAKHALIN	NORS	0.220
S14	96120	71	9	6	5	45	59	46.4	N	141.1	E	16	5.7	SAKHALIN	NOAA	0.082
S15	97660	71	9	6	20	10	47	46.5	N	141.2	E	N	5.0	SAKHALIN	NOAA	0.220
S16	3340	71	9	8	3	17	25	46.7	N	141.3	E	16	5.0	SAKHALIN	NOAA	0.300
S20	4470	71	9	8	11	43	23	46.4	N	141.1	E	6	5.9	SAKHALIN	NOAA	0.096
S21	4760	71	9	8	12	33	55	46.4	N	141.0	E	19	5.2	SAKHALIN	NOAA	0.050

CODE	EPX	Y	M	D	H	M	S	LAT		LONG		D	MB	REGION	SOURCE	LTM
S22	5690	71	9	8	16	59	52	45.3	N	140.9	E	16	5.9	SAKHALIN	NOAA	0.070
S23	6290	71	9	8	19	22	15	45.4	N	140.9	E	19	5.3	SAKHALIN	NOAA	0.080
---	EVENT SET - KURILES															
KJ01	66770	72	12	10	18	25	7	44.8	N	149.4	E	13	6.0	KURILES	NOAA	0.465
KJ02	67410	72	12	11	0	22	20	44.8	N	149.2	E	30	4.8	KURILES	NOAA	0.805
KJ03	67760	72	12	11	2	5	19	44.7	N	149.4	E	N	4.3	KURILES	NOAA	0.741
KJ04	69410	72	12	11	15	13	45	44.8	N	149.3	E	N	4.3	KURILES	NOAA	0.883
KJ05	69640	72	12	11	19	32	52	44.7	N	149.3	E	45	4.8	KURILES	NOAA	1.016
KJ06	75800	72	12	15	18	41	31	44.6	N	149.4	E	40	4.7	KURILES	NOAA	0.827
KJ07	79510	72	12	17	0	13	33	44.7	N	149.2	E	50	5.7	KURILES	NOAA	0.380
KJ08	79570	72	12	17	0	32	22	44.7	N	149.3	E	N	4.8	KURILES	NOAA	0.863
KJ09	79680	72	12	17	1	13	15	44.8	N	149.2	E	N	4.7	KURILES	NOAA	0.883
KJ10	79770	72	12	17	1	26	4	44.7	N	149.4	E	N	4.8	KURILES	NOAA	0.745
KJ11	80460	72	12	17	5	45	57	44.7	N	149.3	E	N	4.6	KURILES	NOAA	0.616
KJ12	80570	72	12	17	6	24	51	44.6	N	149.4	E	N	4.1	KURILES	NOAA	0.502
---	EVENT SET - SOUTH OF HONSHU															
HJ01	68680	72	12	11	9	10	27	33.2	N	141.0	E	N	4.1	SOUTH OF HONSHU	NOAA	0.480
HJ02	72500	72	12	13	6	29	55	33.3	N	141.0	E	41	4.2	SOUTH OF HONSHU	NOAA	0.533
HJ03	73740	72	12	14	12	25	9	32.9	N	141.0	E	22	4.2	SOUTH OF HONSHU	NOAA	0.093
HJ04	73850	72	12	14	13	50	19	33.2	N	141.0	E	41	4.6	SOUTH OF HONSHU	NOAA	0.328
HJ05	75080	72	12	15	6	7	43	33.0	N	141.0	E	39	3.9	SOUTH OF HONSHU	NOAA	0.561
HJ06	75150	72	12	15	6	15	20	33.3	N	141.3	E	35	5.2	SOUTH OF HONSHU	NOAA	0.228
HJ07	84260	72	12	18	16	23	53	33.2	N	140.8	E	43	4.3	SOUTH OF HONSHU	NOAA	0.572
HJ08	84730	72	12	18	23	27	2	33.3	N	140.8	E	8	4.6	SOUTH OF HONSHU	NOAA	0.548
HJ09	85400	72	12	19	6	0	25	33.2	N	140.9	E	36	4.2	SOUTH OF HONSHU	NOAA	0.324
---	EVENT SET - EASTERN KAZAKH (E)															
512	31850	71	6	30	3	56	57	50.0	N	79.1	E	0	5.4	EASTERN KAZAKH SSR	NOAA	0.820
EK02	92390	72	6	7	1	27	55	49.8	N	78.2	E	0	5.5	EASTERN KAZAKH SSR	NOAA	1.080
513	15320	71	10	21	6	2	57	50.0	N	77.6	E	0	5.6	EASTERN KAZAKH SSR	NOAA	0.980
EK03	56339	71	10	9	6	2	56	50.0	N	77.7	E	0	5.4	EASTERN KAZAKH SSR	NOAA	1.060
EK04	25570	71	12	15	7	53	52	50.0	N	77.9	E	0	4.9	EASTERN KAZAKH SSR	NOAA	1.080
511	13038	71	6	6	3	2	57	50.0	N	77.8	E	0	5.5	EASTERN KAZAKH SSR	NOAA	0.960
EK05	6030	72	3	29	3	4	17	46.5	N	76.0	E		3.8	EASTERN KAZAKH SSR	NORS	0.800
EK06	24740	71	6	19	4	3	0	50.0	N	77.7	E	0	5.5	EASTERN KAZAKH SSR	NOAA	1.010
EK07	35020	72	2	10	5	2	57	50.0	N	78.0	E	0	5.5	EASTERN KAZAKH SSR	NOAA	0.630

CODE	EPX	Y	M	D	H	I	S	LAT		LONG		D	MB	REGION	SOURCE	LTM
514		71	12	30	6	20	58	49.9	N	78.1	E	0	5.8	EASTERN KAZAKH SSR	NOAA	0.938
EK08	657	72	5	25	4	2	0	49.8	N	78.2	E	0	5.2	EASTERN KAZAKH SSR	NOAA	1.136
515		72	3	10	4	56	57	49.8	N	78.2	E	0	5.5	EASTERN KAZAKH SSR	NOAA	0.858
516		72	3	28	4	21	57	49.7	N	78.2	E	0	5.2	EASTERN KAZAKH SSR	NOAA	0.927
517		72	7	6	1	2	58	49.7	N	78.0	E		4.4	EASTERN KAZAKH SSR	NOAA	1.023
518		72	12	28	4	26	58	50.0	N	79.0	E		4.2	EASTERN KAZAKH SSR	NORS	0.913
519		72	10	26	4	47	35	49.0	N	77.0	E		3.9	EASTERN KAZAKH SSR	NORS	0.946
---	EVENT SET - CENTRAL ASIA															
102		71	6	15	22	4	13	41.5	N	79.3	E	N	5.6	KIRGIZ-SINKIANG BORDER	NOAA	0.650
103		71	6	16	0	58	37	41.5	N	79.4	E	N	5.4	KIRGIZ-SINKIANG BORDER	NOAA	0.530
104		71	6	19	17	23	3	41.5	N	71.3	E	N	5.2	KIRGIZ-SINKIANG BORDER	NOAA	0.568
105		71	7	24	11	43	29	39.5	N	73.2	E	N	5.6	TADZHIK-SINKIANG BORDER	NOAA	0.250
106		71	7	26	1	48	34	39.9	N	77.2	E	N	6.0	SOUTHERN SINKIANG CHINA	NOAA	0.097
107		71	10	28	13	30	57	41.9	N	72.4	E	22	5.5	KIRGIZ SSR	NOAA	0.281
108		72	1	2	10	27	35	41.8	N	84.5	E	N	5.2	SOUTHERN SINKIANG CHINA	NOAA	0.492
109		72	1	15	20	21	50	40.3	N	79.0	E	N	5.4	SOUTHERN SINKIANG CHINA	NOAA	0.306
111		71	11	8	3	6	36	27.1	N	54.5	E	36	5.6	SOUTHERN IRAN	NOAA	0.348
112		72	1	14	22	10	4	32.8	N	46.0	E	N	5.1	IRAN-IRAQ BORDER REGION	NOAA	0.519
113		72	2	26	23	31	10	50.6	N	97.3	E	N	5.3	USSR-MONGOLIA BORDER	NOAA	0.181
226		72	3	15	6	0	32	30.4	N	84.5	E	N	5.3	TIBET	NOAA	0.566
227		72	4	5	22	38	36	38.4	N	73.5	E	118	5.0	TADZHIK-SINKIANG BORDER	NOAA	0.193
229		72	4	20	0	35	56	42.0	N	84.6	E	N	5.1	NORTHERN SINKIANG PROV.	NOAA	1.006
230		72	4	28	0	52	56	31.3	N	84.0	E	N	5.1	TIBET	NOAA	0.316
---	EVENT SET - WESTERN RUSSIA (E)															
WR01	00119	72	6	16	12	20	53	570.0	N	470.0	E		3.2	WESTERN RUSSIA	NORS	1.360
WR03	57777	72	7	9	7	0	8	520.0	N	310.0	E		4.6	WESTERN RUSSIA	LASA	1.340
WR04	75059	71	9	19	10	59	15	57.8	N	41.1	E	N	4.5	WESTERN RUSSIA	NOAA	1.360
WR05	31629	71	10	4	9	59	54	61.6	N	47.1	E	13	5.1	WESTERN RUSSIA	NOAA	1.160
WR06	48360	71	7	10	17	0	4	64.2	N	55.2	E	0	5.3	URAL MOUNTAINS REGION	NOAA	0.960
WR07	20560	71	10	22	5	0	2	51.6	N	54.5	E	6	5.3	WESTERN RUSSIA	NOAA	0.840
---	EVENT SET - WESTERN KAZAKH (E)															
WK01	95809	72	7	31	14	21	21	50.0	N	46.0	E		3.9	WESTERN KAZAKH SSR	LASA	0.720
WK02	97530	72	7	14	14	58	36	51.0	N	47.0	E		3.7	WESTERN KAZAKH SSR	LASA	0.830
WK03	75848	72	7	11	7	20	42	50.0	N	47.0	E		3.8	WESTERN KAZAKH SSR	LASA	0.870
WK05	48289	71	12	22	6	59	45	47.9	N	48.2	E	0	6.0	WESTERN KAZAKH SSR	NOAA	0.880

CODE	EPx	Y	M	D	H	I	S	LAT		LONG		D	MB	REGION	SOURCE	LTM
---	EVENT SET - CAUCASUS															
	39680	71	10	15	17	7	51	41.4	N	48.6	E		N 4.9	EASTERN CAUCASUS	NOAA	0.950
	23720	72	2	3	2	20	56	40.7	N	48.4	E	39	5.1	EASTERN CAUCASUS	NOAA	0.450
---	EVENT SET - CRIMEA															
	55908	72	7	22	5	10	45	44.9	N	36.0	E		N 4.6	CRIMEA REGION	NOAA	0.740
---	EVENT SET - GREECE															
GR01	37588	72	7	18	13	45	38	41.6	N	23.8	E		N 4.0	GREECE-BULGARIA BORDER	NOAA	0.400
	23670	72	9	21	2	22	0	38.0	N	20.3	E		N 4.0	GREECE	NOAA	0.570
	32560	71	10	4	15	35	52	34.4	N	26.1	E	33	4.8	GRETE	NOAA	0.720
	87320	72	1	10	15	12	47	35.1	N	27.7	E	42	4.1	DODECANESE ISLANDS	NOAA	0.600
	90179	72	1	12	13	51	49	35.0	N	23.5	E	48	4.9	GRETE	NOAA	0.630
	51900	72	2	20	21	38	48	36.8	N	21.6	E	55	4.4	SOUTHERN GREECE	NOAA	0.970
	87348	72	6	1	13	44	24	40.0	N	23.0	E		3.4	GREECE	NORS	0.430
	53100	72	7	5	18	5	12	36.9	N	21.5	E	17	4.7	SOUTHERN GREECE	NOAA	0.650
	53220	72	7	5	19	8	45	37.6	N	20.6	E		N 3.8	IONIAN SEA	NOAA	0.530
	59499	72	7	8	5	46	28	41.6	N	23.6	E	28	4.7	GREECE-BULGARIA BORDER	NOAA	0.420
	9570	72	3	31	2	58	19	36.5	N	21.2	E		N 4.7	SOUTHERN GREECE	NOAA	0.450
	77029	72	5	23	3	14	48	41.7	N	23.6	E	5	4.3	GREECE-BULGARIA BORDER	NOAA	0.460
	62880	72	12	9	8	51	47	38.3	N	20.2	E	21	4.7	GREECE	NOAA	0.520
	46230	72	12	2	13	23	21	35.4	N	27.1	E	55	5.1	DODECANESE ISLANDS	NOAA	0.750
	50880	72	12	4	3	25	31	35.2	N	27.2	E	39	4.3	DODECANESE ISLANDS	NOAA	0.800
	54400	72	12	5	12	0	20	39.0	N	23.9	E	62	4.7	AEGEAN SEA	NOAA	0.029
	74220	72	7	25	1	56	25	38.7	N	21.4	E	45	4.5	GREECE	NOAA	0.210
	98639	72	6	15	0	34	8	38.3	N	22.2	E	26	4.9	GREECE	NOAA	0.104
	73640	72	10	4	8	48	28	38.3	N	20.2	E		N 4.8	GREECE	NOAA	0.280
---	EVENT SET - TURKEY															
	4680	72	8	3	21	39	40	37.7	N	32.7	E	41	4.5	TURKEY	NOAA	0.280
	73430	72	10	4	5	14	33	39.1	N	27.4	E		N 4.4	TURKEY	NOAA	0.270
	89310	72	9	3	8	33	28	39.2	N	28.1	E	16	4.6	TURKEY	NOAA	0.110
	72050	72	7	24	10	22	0	39.4	N	40.1	E		N 4.4	TURKEY	NOAA	0.220
	10730	72	7	16	2	47	26	38.3	N	43.3	E	40	4.9	TURKEY	NOAA	0.100
	14390	71	8	17	4	30	23	37.1	N	36.8	E		N 5.0	TURKEY	NOAA	0.220
	50630	72	2	28	2	5	3	40.4	N	29.1	E	6	4.1	TURKEY	NOAA	0.280
	23270	71	10	3	7	44	35	38.9	N	29.0	E	23	4.7	TURKEY	NOAA	0.090
	39130	71	7	5	16	53	52	41.9	N	32.5	E	6	4.3	TURKEY	NOAA	0.190

CODE	EPX	Y	M	D	H	I	S	LAT		LONG		D	MB	REGION	SOURCE	LTM
---	EVENT SET - YUGOSLAVIA															
	60620	72	10	1	4	30	52	43.5	N	21.5	E	3	4.9	YUGOSLAVIA	NOAA	0.13
---	EVENT SET - ITALY															
IT01	53160	71	7	15	1	33	1	44.8	N	10.3	E	8	5.2	NORTHERN ITALY	NOAA	0.18
IT02	32590	71	10	4	15	43	27	42.9	N	13.1	E	N	5.0	CENTRAL ITALY	NOAA	0.06
IT03	27180	72	2	5	1	26	29	43.2	N	13.3	E	N	4.8	CENTRAL ITALY	NOAA	0.02
IT04	29310	72	2	6	1	34	18	44.0	N	13.2	E	N	4.9	ADRIATIC SEA	NOAA	-.11
IT05	98550	72	6	14	21	1	11	43.7	N	13.8	E	6	4.7	CENTRAL ITALY	NOAA	0.12
IT06	98480	72	6	14	18	55	55	43.7	N	13.4	E	14	4.9	CENTRAL ITALY	NOAA	-0.30
---	EVENT SET - GIBRALTAR															
	59940	72	2	27	12	13	47	34.8	N	9.1	W	N	4.7	WEST OF GIBRALTAR	NOAA	-0.08
---	EVENT SET - MID-ATLANTIC RIDGE															
223		71	8	3	5	34	26	23.4	N	39.2	W	N	5.0	NORTH ATLANTIC RIDGE	NOAA	-0.18
222		71	9	22	5	29	49	31.1	N	41.6	W	N	4.8	NORTH ATLANTIC RIDGE	NOAA	-0.16
225		71	11	21	15	5	37	23.9	N	45.0	W	N	4.8	NORTH ATLANTIC RIDGE	NOAA	-0.28
220		71	11	22	22	40	2	30.1	N	42.7	W	N	5.2	NORTH ATLANTIC RIDGE	NOAA	-0.03
224		72	2	5	4	18	42	14.5	N	45.1	W	N	5.0	NORTH ATLANTIC RIDGE	NOAA	-0.49
---	EVENT SET - WEST COAST OF NORTH AMERICA															
301		71	7	8	14	0	0	37.1	N	116.1	W	0	5.5	SOUTHERN NEVADA	NOAA	0.01
302		71	11	20	21	24	43	48.8	N	129.5	W	N	5.5	VANCOUVER ISLAND REGION	NOAA	-0.45
303		71	12	5	5	50	6	49.5	N	129.5	W	5	5.6	VANCOUVER ISLAND REGION	NOAA	-0.37
304		71	7	12	9	2	9	24.0	N	111.2	W	N	4.8	BAJA CALIFORNIA	NOAA	-0.02
305		72	1	13	21	59	49	22.7	N	107.9	W	N	5.0	COAST OF CENTRAL MEXICO	NOAA	-0.21
306		72	2	20	6	8	18	29.9	N	113.5	W	N	5.4	GULF OF CALIFORNIA	NOAA	-0.08
307		0	4	8	6	24	18	42.6	N	126.3	W	11	5.6	OFF COAST OF OREGON	NOAA	-0.10
---	EVENT SET - NEVADA (E)															
	45640	71	7	8	14	0	8	37.1	N	116.1	W	0	5.5	NEVADA	NOAA	0.22
	31650	71	6	29	18	30	21	40.1	N	116.1	W		4.4	NEVADA	NORS	0.32
	24150	71	12	14	21	10	11	37.1	N	116.1	W	0	4.0	NEVADA	NOAA	0.46
	71940	72	5	19	17	0	7	37.0	N	116.0	W	0	4.9	NEVADA	NOAA	0.50
	51760	72	7	20	17	15	0	37.2	N	116.2	W	0	5.0	NEVADA	NOAA	0.18
	25040	72	9	21	15	30	5	37.1	N	116.0	W	0	5.4	CALIFORNIA-NEVADA BORDER	NOAA	-0.19
---	EVENT SET - UTAH/DAKOTA															
	64020	72	10	1	0	0	0	40.9	N	109.3	W		3.8	UTAH	NORS	0.30
	74985	72	1	3	10	20	46	38.5	N	112.1	W	5	4.6	UTAH	NOAA	0.60

CODE	EPX	Y	M	D	H	M	S	LAT		LONG		D	MB	REGION	SOURCE	LTM
	73139	72	8	29	1	35	39	25.4	N	109.8	W	N	4.8	NW. MEXICO	NOAA	-0.400
	61350	72	12	8	0	0	0	44.6	N	102.2	W		3.7	SOUTH DAKOTA	NDRS	0.050
---	EVENT SET - GULF OF CALIFORNIA															
	50500	72	2	20	2	32	19	30.0	N	113.6	W	N	4.2	GULF OF CALIFORNIA	NOAA	-0.050
	50910	72	2	20	6	9	27	29.9	N	113.5	W	N	5.4	GULF OF CALIFORNIA	NOAA	-0.100
	51420	72	2	20	13	2	10	29.7	N	113.4	W	N	4.3	GULF OF CALIFORNIA	NOAA	-0.010
	52320	72	2	21	4	51	26	29.7	N	113.5	W	N	4.8	GULF OF CALIFORNIA	NOAA	-0.030
	52430	72	2	21	7	0	46	30.0	N	113.6	W	N	4.9	GULF OF CALIFORNIA	NOAA	-0.170
---	SOME ADDITIONAL LARGE EVENTS															
122		71	11	06	22	00	00	51.4	N	179.1	E	2	6.8	ALEUTIANS (expl.)	NOAA	
123		72	03	20	23	31	48	51.3	N	179.2	W	46	6.0	ALEUTIANS	NOAA	
124		72	06	24	15	29	22	36.2	N	69.7	E	47	6.0	HINDU KUSH	NOAA	

REFERENCES

1. Haskell, N.A., "Total energy and energy spectral density of elastic wave radiation from propagating faults", Bull. Seism.Soc.Am., Vol. 54, pp. 1811-1841 (December 1964).

2. Haskell, N.A., "Total energy and energy spectral density of elastic wave radiation from propagating faults. Part II. A statistical source model", Bull.Seism.Soc.Am.,Vol. 56, pp. 124-140 (February 1966).

3. Savage, J.C., "Radiation from a realistic model of faulting", Bull.Seism.Soc.Am., Vol. 56, pp. 577-592 (April 1966).

4. Aki, K., "Scaling law of seismic spectrum", Jour.Geophys. Res., Vol. 72, pp. 1217-1231 (February 1967).

5. Brune, J.N., "Tectonic stress and the spectra of seismic shear waves from earthquakes", Jour.Geophys.Res., Vol. 75 pp. 4997-5009 (September 1970).

6. Seggern, D.von and R.Blandford, "Source time functions and spectra for underground nuclear explosions", Geophys.J.R. astr.Soc., Vol. 31, pp. 83-97 (December 1972).

7. Wyss,M., T.C.Hanks and R.C.Liebermann, "Comparison of P-wave spectra of nuclear explosions and earthquakes", Jour. Geophys.Res., Vol. 76, pp. 2716-2729 (April 1971).

8. Hanks, T.C. and M.Wyss, "The use of body-wave spectra in the determination of seismic source parameters", Bull.Seism. Soc.Am., Vol. 62, pp. 561-589 (April 1972).

   Wyss, M. and T.C. Hanks, "The source parameters of the San Fernando earthquake inferred from teleseismic body waves", Ibid., pp. 591-602.

9. Briscoe,B., Seismic Discrimination, Semiannual Technical Summary Report, Lincoln lab., M.I.T., p. 5 (June 1967).

10. Kelly, E.J., "A study of two short-period discriminants", Technical Note 1968-8, Lincoln lab., M.I.T. (April 1969).

11. Lacoss, R.T.,"A large-population LASA discrimination experiment", Technical Note 1969-24, Lincoln lab., M.I.T. (April 1969).

12. Mohajeri, M., "Statistics of the spectral ratio and log-likelihood ratio seismic discriminants", Technical Note 1971-33, Lincoln lab., M.I.T. (September 1971).

13. Anglin, F.M., "Discrimination of earthquakes and explosions using short period seismic array data", Nature, Vol.233, pp. 51-52 (September 1971).

14. Israelson, H., "Seismic identification using short period Hagfors data", FOA-4 Report C4468-26, Research Inst. of National Defence, Sweden (1971).

15. Lacoss, R.T. and G.T.Kuster, "Processing a partially coherent large seismic array for discrimination", Technical Note 1970-30, Lincoln lab., M.I.T. (November 1970).

16. Noponen, I.T., E.S.Husebye and D.Rieber-Mohn, "Extraction of P wave spectra using the NORSAR array", Proc.Sem.Seismology and Seismic Arrays, Oslo 22-25 Nov. 1971, ed. by E.S.Husebye and H.Bungum, NORSAR, Kjeller (P.O.Box 51), Norway (September 1972).

17. Linde, A.T. and I.S. Sacks, "Errors in the spectral analysis of long-period body waves", Jour.Geophys.Res., Vol.76, pp. 3326-3336 (May 1971).

18. Filson, J.R., "On estimating explosive source parameters at teleseismic distances", Technical Note 1970-9, Lincoln lab., M.I.T.(July 1970).

19. Kulhanék, O., Source parameters of some presumed Semipalatinsk underground nuclear explosions", Pure and Applied Geoph., Vol. 102, pp. 51-66 (1973).

20. Zander, I. and R. Araskog, "Nuclear explosions 1945-1972, basic data", FOA-4 Report A 4505-A1, Research Inst. of National Defence, Sweden (April 1973).

21. Fuchs, K., "The transfer function for P-waves for a system consisting of a point source in a layered medium", Bull. Seism.Soc.Am., Vol. 56, pp. 75-108 (February 1966).

22. Bendat, J.S. and A.G.Piersol, "Spectral density function estimates", Chapter 6, Random data: Analysis and Measurement Procedures, John Wiley & Sons, Inc. (1971).

23. Bracewell, R., " Moments", Chapter 8, The Fourier Transform and its Applications, McGraw-Hill Book Company Inc.(1965).

24. Weichert, D.H., "Short-period spectral discriminant for earthquake-explosion differentiation", Zeitschrift f. Geophysik, Vol. 37, pp. 147-152 (1971).

25. Basham, P.W., "Canadian magnitudes of earthquakes and nuclear explosions in south-western North America", Geophys. J.R.astr.Soc., Vol. 17, pp. 1-13 (January 1969).

26. Solomon, S.C. and M.N.Toksöz, "Lateral variation of attenuation of P and S waves beneath the United States", Bull. Seism.Soc.Am., Vol. 60, pp. 819-838 (June 1970).

27. Solomon, S.C., "On Q and seismic discrimination", Geophys. J.R.astr.Soc., Vol. 31, pp. 163-177 (December 1972).

28. Manchee, E.B., "Short period seismic discrimination",Nature, Vol. 239, pp. 152-153 (September 1972).

29. Dahlman,O., H.Israelson, A.Austegard and G.Hörnström, "Definition and identification of seismic events in the USSR in 1971", FOA 4 Report C 4540-A1, Research Inst. of National Defence, Sweden (June 1973).

30. Israelson,H., "Variability of short period discriminants obtained at the Hagfors Observatory from Eurasian events", manuscript, Research Inst. of National Defence, Sweden (March 1973).

31. Randall, M.J., "The spectral theory of seismic sources", Bull.Seism.Soc.Am., Vol.63, pp. 1133-1144 (June 1973).

32. Müller, G., "Seismic moment and long-period radiation of underground nuclear explosions", Bull.Seism.Soc.Am., Vol. 63, pp. 847-857 (June 1973).

33. Davies,D. (Rapporteur), "Seismic Methods for Monitoring Underground Explosions", Report by a Seismic Study Group, SIPRI (International Institute for Peace and Conflict Research, Sveavägen 166, Stockholm, Sweden), p. 83 (August 1968).

34. Vinnik, L.P. and A.A. Godzikovskaya, "Sounding of the Earth's mantle by the method of seismically conjugate points", Bull.(Izv.) Acad.Sci.USSR, Phys. of the Solid Earth, English Ed., No. 10, 1972, pp. 656-664 (April 1973).